



Assessment of the sensitivity of model responses to urban emission changes in support of emission reduction strategies

Bertrand Bessagnet¹ · Kees Cuvelier¹ · Alexander de Meij² · Alexandra Monteiro³ · Enrico Pisoni¹ · Philippe Thunis¹ · Angelos Violaris⁴ · Jonilda Kushta⁴ · Bruce R. Denby⁵ · Qing Mu⁵ · Eivind G. Wærsted⁵ · Marta G. Vivanco⁶ · Mark R. Theobald⁶ · Victoria Gil⁶ · Ranjeet S. Sokhi⁷ · Kester Momoh⁷ · Ummugulsum Alyuz⁷ · Rajasree VPM⁷ · Saurabh Kumar⁷ · Elissavet Bossioli⁸ · Georgia Methymaki⁸ · Darijo Brzolja⁹ · Velimir Milić⁹ · Arineh Cholakian¹⁰ · Romain Pennel¹⁰ · Sylvain Mailler¹⁰ · Laurent Menut¹⁰ · Gino Briganti¹¹ · Mihaela Mircea¹¹ · Claudia Flandorfer¹² · Kathrin Baumann-Stanzer¹² · Virginie Hutsemékers¹³ · Elke Trimpeneers¹³

Received: 5 April 2023 / Accepted: 7 November 2023 / Published online: 26 December 2023
© The Author(s) 2023

Abstract

The sensitivity of air quality model responses to modifications in input data (e.g. emissions, meteorology and boundary conditions) or model configurations is recognized as an important issue for air quality modelling applications in support of air quality plans. In the framework of FAIRMODE (Forum of Air Quality Modelling in Europe, <https://fairmode.jrc.ec.europa.eu/>) a dedicated air quality modelling exercise has been designed to address this issue. The main goal was to evaluate the magnitude and variability of air quality model responses when studying emission scenarios/projections by assessing the changes of model output in response to emission changes. This work is based on several air quality models that are used to support model users and developers, and, consequently, policy makers. We present the FAIRMODE exercise and the participating models, and provide an analysis of the variability of O₃ and PM concentrations due to emission reduction scenarios. The key novel feature, in comparison with other exercises, is that emission reduction strategies in the present work are applied and evaluated at urban scale over a large number of cities using new indicators such as the absolute potential, the relative potential and the absolute potency. The results show that there is a larger variability of concentration changes between models, when the emission reduction scenarios are applied, than for their respective baseline absolute concentrations. For ozone, the variability between models of absolute baseline concentrations is below 10%, while the variability of concentration changes (when emissions are similarly perturbed) exceeds, in some instances 100% or higher during episodes. Combined emission reductions are usually more efficient than the sum of single precursor emission reductions both for O₃ and PM. In particular for ozone, model responses, in terms of linearity and additivity, show a clear impact of non-linear chemistry processes. This analysis gives an insight into the impact of model sensitivity to emission reductions that may be considered when designing air quality plans and paves the way of more in-depth analysis to disentangle the role of emissions from model formulation for present and future air quality assessments.

Keywords Modelling · Air quality · Emission projections · Policy support · Model sensitivity

Introduction

Improving air quality is not only beneficial for human health, but it also reduces our impact on climate change (EEA 2020; Feng and Fang 2022). Therefore, actions to reduce air pollutant emissions can have multiple benefits. Air quality models, such as chemistry transport models (CTM), are valuable tools for

the assessment of the impact of emission reduction strategies and forecasting of pollutant concentrations. Since models are being progressively used for policy support, such as in the frame of the Air Convention or the Ambient Air Quality Directive (EU 2008), model performance and response sensitivity assessment have become an increasingly important issue.

Although many studies tackle the impact of chemical and physical processes, initial and boundary conditions, or emissions on absolute concentrations or trends (Curci 2012; de Meij et al. 2009; Dufour et al. 2021; Huang et al. 2020; Huertas et al. 2021; Khan and Kumar 2019; Li et al. 2021;

Kees Cuvelier retired with Active Senior Agreement.

Extended author information available on the last page of the article

Pernigotti et al. 2012; Thunis et al. 2021b; Vuolo et al. 2009; Yan et al. 2021), dedicated exercises to evaluate the variability of model responses (concentration changes) to local emission modifications are not common. It is however a key element to ensure robust policymaking, since absolute or relative concentration changes are commonly used to estimate or evaluate the efficiency of air quality plans, particularly in the frame of integrated assessment tools (Viaene et al. 2016).

Long-term modelling exercises such as EURODELTA (Bessagnet et al. 2016; Ciarelli et al. 2019; Colette et al. 2017; Mircea et al. 2019; Thunis et al. 2010; Vivanco et al. 2017), AQMEII (Im et al. 2018; Liu et al. 2018; Solazzo et al. 2012, 2013) and CityDelta (Cuvelier et al. 2007; Thunis et al. 2007; Vautard et al. 2007) were designed to evaluate and intercompare model responses to emission changes. With the exception of Citydelta, these exercises mostly focused on continental and regional model responses.

FAIRMODE is the Forum of Air Quality Modelling in Europe aiming at bringing together air quality modellers and users in order to promote and support the harmonized use of models (Miglietta et al. 2012; Monteiro et al. 2018; Kushta et al. 2019; Pisoni et al. 2019), with emphasis on model application under the European Air Quality Directive. In the context of FAIRMODE, a dedicated intercomparison exercise has been formulated to assess the sensitivity of model responses to emission changes, with the view of assessing and understanding the main causes of discrepancies between models.

The current work refers to an intercomparison platform, rather than an intercomparison exercise, to reflect the fact that the activity is continuous, in contrast to intercomparison exercises previously cited, that took place over a defined period of time. At the current stage of this long-term programme, the goal of this paper is not to provide an in-depth analysis, but rather accentuate the diversity of model responses and identify what processes could be potential drivers of this variability. The objective of this paper is twofold: (i) present the FAIRMODE platform and models involved as a community initiative, and (ii) evaluate the amplitude of the model responses for O₃ and PM concentrations, two pollutants that are formed or partially formed in the atmosphere, respectively.

Design of the intercomparison platform

Overall framework and setup

The focus of this benchmarking platform is on the urban and regional (i.e. sub-national) scales. The setup considers a range of European cities (mostly EU capitals) plus a few larger regions with high levels of pollution. The proposed geographical distribution ensures adequate coverage of Europe to take into account the diversity of atmospheric conditions, meteorological particularities and emissions. Theoretical emission changes

are applied on the entire urban (i.e. the large functional urban area as defined by the OECD (OECD 2012) or regional area (e.g. the administrative region). Note that, as initially designed, the platform is well suited to modelling systems from regional to urban scales (i.e. it does not address fine scale traffic site environments or industrial hot spots). By “modelling system”, we refer here to the system composed by the air quality model itself (configured with chemical/aerosol schemes, transport and dispersion algorithms, models for natural emissions of gas and aerosol, etc.) and its associated input data (anthropogenic emissions, meteorology, initial and boundary conditions, etc.) at all relevant spatial scales. By “responses to emission changes”, we mean the concentration change (or delta) resulting from a given reduction of emissions from anthropogenic activities.

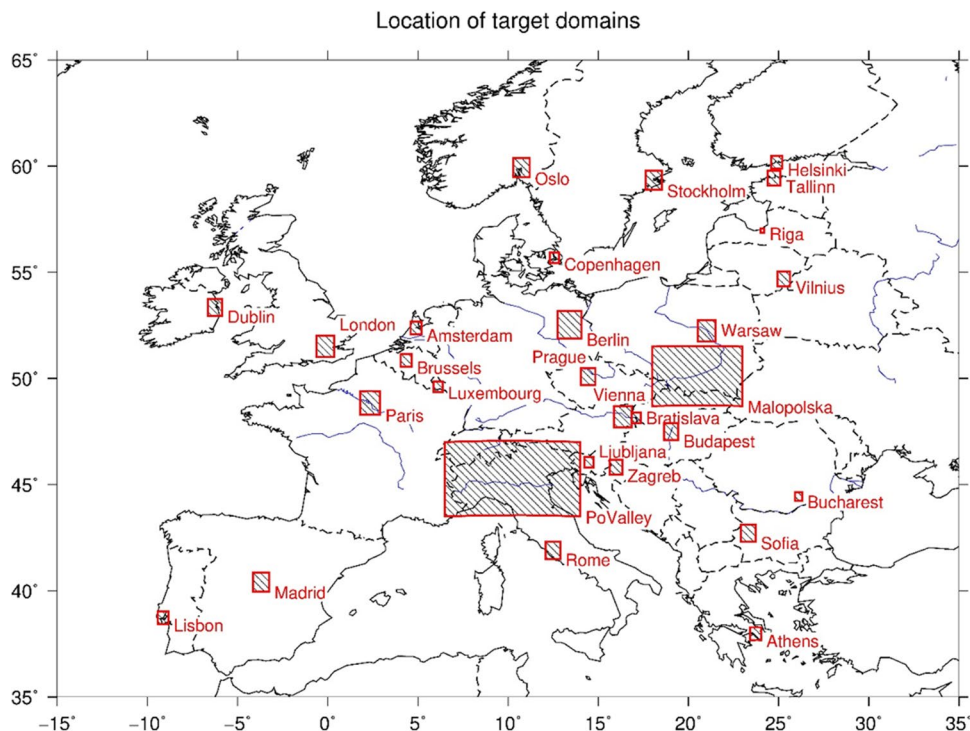
Both short-term (ST) episodes and long-term (LT) simulations are considered. Given their limited CPU demand, ST episodes allow users to perform simulations for a larger number of scenarios focusing on mechanisms and processes that favour such conditions. Assessment of ST episodes also provides information on specific timeframes with threshold exceedances or unusually high concentrations, while LT simulations do not address as they focus on long-term consistency and benefits as well as on air quality indicators. In ST cases, a large number of cities can also be considered in a single simulation as city interactions are less likely to occur over a limited episode than over longer time periods. In addition, episodes are easier to analyze and interpret than yearly averages that sometimes include “compensation” processes. On the other hand, episodes generally lead to weaker signals, which might hinder the analysis whereas yearly average concentrations are the most relevant output in the context of the Ambient Air Quality Directives (EU 2008).

For ST episodes, both winter (mostly for particulate matter (PM)) and summer (mostly for ozone (O₃)) episodes were selected. Each episode covers a few days and has been selected based on the CAMS (Copernicus Atmospheric Monitoring Service) reports and observational data from the EEA (European Environmental Agency) air quality e-reporting (AIRBASE 2022). For LT simulations, emission reductions are applied to cities that are far away from each other to avoid reductions applied over one city or region influencing the background levels in another city/region.

As shown in Fig. 1, most cities are EU capitals and two large regions over the North of Italy (Po Valley) and the south of Poland (Malopolska) are selected to extend the analysis to important regional hot spots in Europe. The focus is on the analysis of ground level PM₁₀, PM_{2.5}, O₃ and NO₂ concentrations. Other species, such as HNO₃, NH₃, HCHO, H₂O₂, SO₂, PM speciation and deposited compounds are also stored for ST episodes to support the analysis but are not a focus of the present study.

To evaluate the diversity of responses in real policy support situations, each modelling group used its own setup and

Fig. 1 Location of the target domains where emission reductions take place



input data (emissions, boundary conditions, meteorology, etc.). Moreover, constraining the sources of meteorological data in such an exercise is not fully relevant because CTM models not online coupled to meteorology often recalculate key variables such as the planetary boundary layer, the vertical eddy diffusion or the vertical wind speed to keep mass conservation, with their own parameterisations. The only constraints are (i) to simulate the same meteorological year 2015 and (ii) to apply fixed emission reductions over the same spatial area (“target domain”) as defined in Fig. 1. Table 10 in Appendix 1 gives the exact locations. Throughout the paper, “pollutant” refers to species produced or emitted in the atmosphere while “precursor” refers to emitted species which can lead to a new pollutant. For instance, O_3 and PM_{10} are considered pollutants while NO_x and VOCs are precursors. The “delta” terminology refers to the differences between a scenario and the base case concentrations.

Selected scenarios

This intercomparison considered two idealized emission scenarios: emissions are reduced by 25% and 50% for two groups of pollutants depending on whether the pollutant targeted for reduction is PM or O_3 . These reduction rates are in line with usual expected emission reductions able to have a substantial impact on concentrations. The use of these two emission reduction ranges allows for the investigation of the linearity of the respective emission reduction. For PM ST and LT simulations, PPM , NO_x , SO_x , NH_3 and VOC precursor emissions are reduced, while for O_3 ST simulations, only reductions of NO_x and VOC precursors are considered.

For ST simulations, emission reductions start at 00:00 UTC the first day and end at 23:00 UTC the last day, while for long-term simulations emission reductions are applied over the entire year. An additional scenario both for LT and ST analyses is performed by reducing all precursors simultaneously, ALL consisting of PPM , NO_x , SO_x , NH_3 and VOC for PM simulations, and ALL referring to NO_x and VOC for ST ozone simulations. This simulation is used to analyze the “additivity” of the effect of emission reductions.

The selection criteria for episodes favour periods that cover several regions and cities at the same time. In terms of air quality, 2015 experienced the highest maximum daily 8-h mean concentrations of O_3 of the last 5 years in Central Europe (EEA 2015). This year was also characterized by elevated PM_{10} annual mean concentrations, and a series of large-scale pollution events affected European air quality throughout the year. For instance, a significant PM_{10} pollution event took place from 12 to 20th February, affecting most areas in Europe. As shown in Bessagnet et al. (2016), emissions from residential heating, including wood and coal combustion, dominate the PM_{10} pollution levels during winter or early spring episodes. The locations or areas selected per each category of simulations (LT/ST) and pollutant (PM and O_3) are summarized in Table 1 (LT), Table 2 (ST/ PM) and Table 3 (ST/ O_3) along the exact time-window of simulations for the episodes studied.

Modelling systems

The models involved in this initiative, as well as the versions of each model, are listed in Table 4. As previously

mentioned, the modelling teams used their own input data and usual model configuration for their local, national or regional applications.

For the simulation of selected episodes, a spin-up period of several days before each episode was performed by all models. For a given model, the initial conditions (meteorology and chemistry) of short-term episodes are the same for the base case and all scenarios. The models simulate an emission reduction over the target domain defined in Table 10 of Appendix 1. However, each model can simulate concentrations over a larger domain encompassing the target domain with an appropriate resolution of at least 0.1°. They can also use a cascade of nested grids to reach the highest resolution

align with specific configuration needs of the respective modelling system. Table 5 summarizes the main characteristics of the modelling systems and shows the diversity of model configurations.

Most models are offline, i.e. chemical species, and, particularly, aerosols do not interact with meteorology through the radiative budget. Only WRF-Chem users have activated the default online option which enables the interaction between aerosols, radiation and clouds through the coupling of chemistry with meteorology in realistic synoptic conditions. The consequence of an activated online coupling is a change of meteorology when emissions and resulting concentrations are modified. This could induce an additional impact on the concentration change according to Cholakian et al. (2023) and highlighted over Europe and Asia in recent works (Bessagnet et al. 2020; Zhou et al. 2018). This effect would be amplified by the fact 4D nudging of large-scale meteorological fields are not activated in any WRF-Chem configuration allowing the local physics to be further modified due to the radiative forcings. Moreover, in some cases, modelling teams in FAIRMODE using CHIMERE or WRF-Chem have delivered results at different spatial resolutions over Paris, Madrid and Athens introducing also grid spacing effects to our results. In Appendix 2, a complete description of the model configurations is provided and in Supplementary material A, the list of models available for a given city/region is provided.

Table 1 List of selected areas for long-term simulations

Country	City/region	Simulation code
Belgium	Brussels	BRU003
Croatia	Zagreb	ZAG009
Germany	Berlin	BER011
Poland	Malopolska	MAL001
Romania	Bucharest	BUC006
Spain	Madrid	MAD004
Sweden	Stockholm	STO008
Italy	Rome	ROM005
Italy	Po Valley	POV002

Table 2 List of selected cities for simulations of short-term PM episodes

Locations			PM episodes in 2015 Emissions reduced by 25% and 50% individually and cumulated (SO _x , VOC, PPM, NO _x , NH ₃)				
			Month				
Country	City	Episode code	JAN	FEB	MAR	APR	JUL
Austria	Vienna	VIE019		10 — 16			
Belgium	Brussels	BRU025				23 — 24	
Czech Republic	Prague	PRA007	1 — 9				
Denmark	Copenhagen	COP028					24 — 26
Finland	Helsinki	HEL029					24 — 26
France	Paris	PAR014		10 — 16			
Germany	Berlin	BER023			15 — 25		
Hungary	Budapest	BUD024			15 — 25		
Ireland	Dublin	DUB026				8 — 10	
Netherlands	Amsterdam	AMS012	1 — 9				
Norway	Oslo	OSL030					24 — 26
Poland	Warsaw	WAR013	1 — 9				
Portugal	Lisbon	LIS010	1 — 9				
Romania	Bucharest	BUC022		2 — 3			
Slovakia	Bratislava	BRA027				22 — 23	
Spain	Madrid	MAD021	22 — 23				
Sweden	Stockholm	STO032					13 — 15
United Kingdom	London	LON020			12 — 21		

Table 3 List of selected cities and areas for simulations of short-term O₃ episodes

Locations			Ozone episodes in 2015 Emissions reduced by 25% and 50% individually and cumulated (VOC, NOx)			
			Month			
Country	City/Region	Episode code	JUN	JUL	AUG	SEP
Austria	Vienna	VIE018			11 — 16	
Belgium	Brussels	BRU034		10 — 17		
Czech Republic	Prague	PRA035		1 — 5		
Denmark	Copenhagen	COP036		24 — 26		
France	Paris	PAR015	5 — 6			
Germany	Berlin	BER037	5 — 6			
Greece	Athens	ATH016		—	6 — 14	
Hungary	Budapest	BUD038			7 — 9	
Ireland	Dublin	DUB039	5 — 6			
Poland	Warsaw	WAR040			7 — 9	
Portugal	Lisbon	LIS041	5 — 6			
Slovakia	Bratislava	BRA042	5 — 6			
Spain	Madrid	MAD043		1 — 5		
United Kingdom	London	LON043		1 — 5		
Poland	Malopolska	MAL045			30 — — 3
Italy	Po Valley	POV046			6 — 14	

Table 4 Institutes/universities and models involved

Institutions	Model	Acronyms of model versions and configurations acronyms
JRC/METCLIM	EMEP	EMEPC2, EMEPC42C, EMEP, EMEPG
GeoSphere Austria	WRF-Chem	WRFZAMG
Met Norway	EMEP + uEMEP	EMEPNO, uEMEPIMP, uEMEPTAG
CyI	WRF-Chem	WRFCYI
NKUA	WRF-Chem	WRFNKUA2A, WRFNKUA6A
DHMZ	ADMS-Urban	ADMS
DHMZ	LOTOS-EUROS	LEDHMZ
LMD	WRF-CHIMEREv2020r1	CHIMLMD03, CHIMLMD10
UH-CACP	WRF-CMAQ	CMAQ
CIEMAT	IFS-CHIMEREv2017r4	CHIMCIE01M, CHIMCIE03M, CHIMCIE09M CHIMCIE27
ENEA	WRF-MINNI	MINNI
IRCELINE	CHIMERE + RIO	RIOCHIRC

Definition of indicators

Several indicators, specifically developed for analyzing modelled concentrations changes in response to emission changes, are selected for the analysis of the results (Thunis et al. 2015; Thunis and Clappier 2014). They include the absolute and relative potential and absolute potency. These indicators are the most suitable for an analysis of potential emissions thanks to a scaling with the reduction intensity and the quantity of reduced emissions, respectively.

The absolute potential (APL) is defined as the difference of concentrations C between a scenario and a base

case normalized by the percentage α of the emission reduction $APL = \Delta C/\alpha$. The relative potential (RPL) is a normalization of the APL by the concentration C_{bc} of the base case: $RPL = \Delta C/\alpha C_{bc}$. The absolute potency APY is the difference of concentrations C between a scenario and a base case normalized by the precursor emission reduction E that has been applied $APY = \Delta C/\alpha E$.

Mean values and average concentrations above the 95th percentile concentration computed over simulated areas (Fig. 1) were used in the analyses. These indicators can be either negative or positive showing a decrease or an increase of concentrations, respectively.

Table 5 Short model description (*formerly known as ZAMG for Zentralanstalt für Meteorologie und Geodynamik)

Model codes	Team name (country)	Model name and version	Large-scale meteo driver and resolution	Emission inventory, resolution, date	Details on domains and resolution
ADMS	DHMZ (HR)	ADMS-Urban	Hourly measurements from local meteo-site “Zagreb-Maksimir” are used for meteo	Croatian National Emission Inventory for Zagreb	Domain covering Zagreb at 500×500 m
CHIMCIE	CIEMAT (ES)	IFS-CHIMEREv2017r4	ECMWF IFS 9 km	EMEP 0.1° + Spanish national inventory, 2015	4 nested domains targeted over Madrid, Paris and Athens with resolutions of 0.27/0.09/0.03/0.01°
CHIMLMD	LMD/IPSL (FR)	WRF-CHIMEREv2020r1	NCEP GFS 1.0°	CAMS-REG V4.2 0.1° 2015	3 nested domains: 30 km/10 km/3 km over Paris
CMAQ	UH-CACP (UK)	WRF and CMAQ	NCEP GFS 0.25°	NAEI 2015 merged with EDGAR V5.0, 2015	2 nested domains 25 km/5 km over London
EMEPC2	JRC (EU)	EMEP rv4.34	ECMWF IFS 9 km	CAMS V2.2.1 0.1°, 2015	Europe 0.1°
EMEPC42C	JRC (EU)	EMEP rv4.34	ECMWF IFS 9 km	CAMS-REG V4.2 + Condensables 0.1° 2015	Europe 0.1°
EMEPE	JRC (EU)	EMEP rv4.34	ECMWF IFS 9 km	EDGAR V5.0 0.1°, 2015	Europe 0.1°
EMEPG	JRC (EU)	EMEP rv4.34	ECMWF IFS 9 km	EMEP 0.1°, 2015	Europe 0.1°
EMEPNO	Met Norway (NO)	EMEP rv4.42	ECMWF IFS 0.1°	EMEP 0.1°, 2015	Europe 0.1°
LEDHMZ	DHMZ (HR)	LOTOS-EUROS	ECMWF IFS 9 km	CAMS-AP-v2.2.1 0.1°, 2015	Europe 0.5°×0.25; Inner: 0.1°×0.05° over Zagreb
MINNI	ENEA (IT)	WRF-MINNI	ECMWF IFS 0.1°	ISPRA Italian national inventory 2015	Po Valley at 4 km
uEMEPIMP uEMEPTAG	Met Norway (NO)	EMEP v4.42 + uEMEP v6.1	ECMWF IFS 0.1°	EMEP 0.1°, 2015	250 m for each city. (Only GNFRs 3, 6 and 7 are modelled at this resolution, the rest at 0.1°)
WRFNKUA	NKUA (GR)	WRF-Chem	NCEP GFS 1.0°	EDGAR-HTAP 0.1°, 2010, monthly emission distributions	Europe 0.5°, Greece 0.056°, Athens 0.019°
WRFZAMG	GeoSphere* Austria (AT)	WRF-Chem	ECMWF IFS 9 km	CAMS-REG v1.1 2015	4 km for Vienna and Po Valley
RIOCHIRC	IRCELINE (BE)	CHI-MEREv2017 + RIOv5.0	ECMWF IFS/JOAQ 0.1°	Belgium Local inventories, 0.5° and 0.1° 2015	Europe with CHIMERE: 0.1×0.1°; Brussels with RIO: 4 km×4 km
WRFCYI	CYI (CY)	WRF-Chem	NCEP GFS 0.5°	EDGAR V5.0 0.1°, 2015	Athens: 20 km/10 km; Po Valley: 30 km/10 km

An additional innovative indicator of variability (VAR) has been defined to obtain a measurable quantity summarizing in an objective way the huge amount of data. It is based on the normal standard deviation of indicators, not only the APL and APY, but it includes also the base case emissions and concentrations for the various model applications. A detailed description of these indicators and explanation of how they are calculated for different domains and scenarios is provided in Appendix 3.

Results and discussion

The variability of individual model performances is provided in supplementary material A and C, for reference, while here are shown the main outcomes of the model responses' intercomparison. Model application performances have been evaluated using available background urban, periurban and rural observations (AIRBASE 2022) for the main pollutants

either for LT or ST simulations. The bias, root mean square error (RMSE) and Pearson's spatiotemporal correlation are used for the evaluation. The evaluation was performed over a common set of stations over each simulation domain.

Regarding the model responses, the results presented hereafter are a summary of the analysis of model outputs in the exercise database, for O_3 and PM_{10} concentrations with respect to emission changes. To support this first snapshot analysis, a complete report of more than 240 figures is provided in supplementary material B in a single document listing the captions of these figures referred as Figure SXXX here. Later in the sections, we refer to few of these figures when needed. The following sections summarize the key findings. A fixed colour code is attributed to each model application. The variability of model responses is examined in terms of amplitude and sign of the concentration changes. Model responses are evaluated over the target domain only (where emission reductions are applied) because it is the common area of all modelling applications.

Models' responses to emission changes: ozone

For LT simulations, the modelled base case O_3 mean concentrations are in the range of 60 to 80 $\mu g m^{-3}$ (Figure S9). For the ST simulations, concentrations above the 95th percentile range from 80 up to 120 $\mu g m^{-3}$ (Figure S18), since the episodes occurred in summer when O_3 concentrations are generally higher.

Focusing on the ST simulations, reducing all precursor emissions at the same time (VOC and NOx) leads, for all models, to a slight increase in O_3 mean concentrations except for large regions like the Po Valley. Looking at individual reductions (NOx and VOC separately), large regions like Po Valley encompassing rural areas depict an overall decrease of O_3 concentrations, on average (Fig. 2 and Figure S35). In the city

of Vienna, the model responses (Figure S13) can have opposite signs depending on model configurations with WRFZAMG simulating a slight decrease and EMEP a slight increase of O_3 concentrations when emission of NOx and VOC are reduced at the same time. Reducing only VOC emissions (Figure S56 and S57) lead as expected to a general reduction of O_3 concentrations. WRFNKUA configurations show a slight increase of ozone concentrations which is impossible to explain directly by chemical processes. However, the WRF-Chem model is an online coupled system, integrating chemical and meteorological processes and their interactions. Thus, there is direct and indirect feedback between the pollutant concentrations and meteorological processes and vice versa. These effects, that cannot be separately quantified, are potentially enough to change the sign of the responses. The largest variability occurs for NOx emission reductions (Figure S35) highlighting the importance of the simulated chemical regime that can differ between cities and models. Over urbanized areas, most models simulate an increase of mean ozone during episodes when applying a combined NOx-VOC emission reduction of 50%. This is explained by the stronger role of NOx in VOC-limited areas where VOC/NOx ratios are the lowest. The classical isopleth diagram depicted in Carter et al. (1982), Dodge (1977) and Oke et al. (2017) shows how NOx emission reductions can provide mixed outcomes depending on the chemical regimes, NOx or VOC limited. Here, we consider average concentrations; however, as shown in Vivanco et al. (2021), the reduction in NOx emissions could lead to opposing effects, depending on the metric considered (SOMO35, AOT40, daily maximum, annual values), that can be more or less influenced by night-time and/or diurnal conditions.

However, over the full year (LT simulation), the mean ozone concentrations increase while the average values exceeding the 95th percentiles decrease over the Po Valley (figures S5-S6)

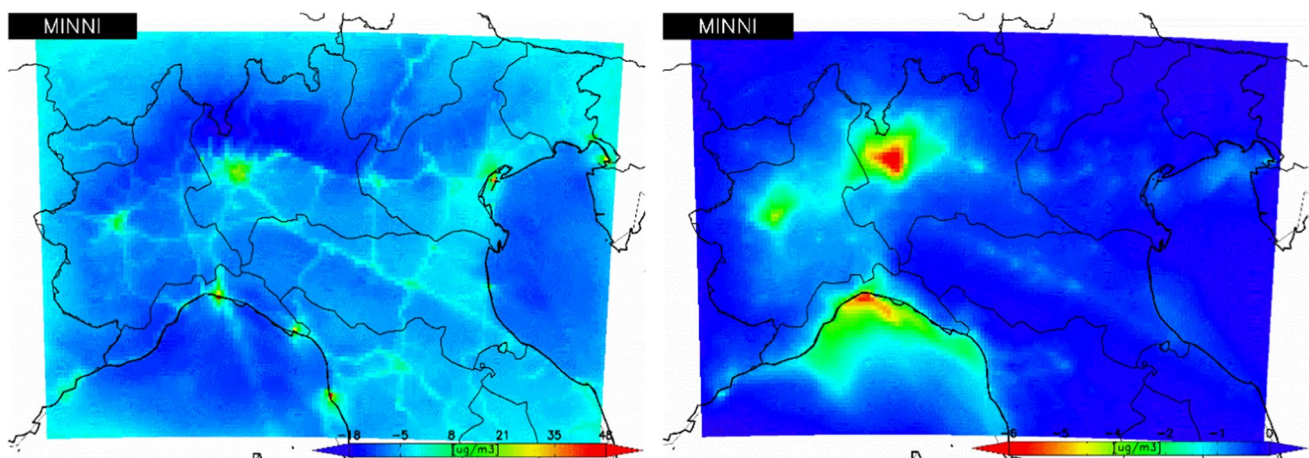


Fig. 2 Example of a graphical output of the benchmark tool showing the absolute potential for ozone comparing a reduction over the Po Valley (from the MINNI model results) of NOx (left) and VOC

(right) emissions. Reducing NOx emissions can increase ozone concentrations within urban areas while VOC emission reductions reduce mean ozone concentrations throughout the domain

if we consider a reduction of both NO_x and VOC emissions. These NO_x/VOC responses applied in large regions are in line with recent studies in Europe (Clappier et al. 2021) and China (Mao et al. 2022) over the Yangtze River Delta Region as well as with (Du et al. 2021) in the central plain in China during the COVID-19 pandemic. As expected, a rather different picture of model responses between rural and urban areas is shown in Fig. 2 for the MINNI results, showing a reduction of mean ozone in both areas when applying VOC emission reductions, and an increase of concentrations over urbanized areas when only NO_x emissions are reduced.

As shown in Fig. 3, for the ST episodes, the reduction of all precursors by 50% leads to different responses in the different locations with varying magnitudes of responses depending on the modelling system. For all models, the lowest absolute potential is displayed for the Warsaw case when reducing all precursors by 50%. The other indicators, relative potential and absolute potency, respond in the same way (Fig. 3). The CHIMERE model applied in Paris and Madrid with different resolutions (light blue, purple and dark blue bars) does not display a large variability in terms of model responses for the relative and absolute potentials for O₃. Over Athens however, the grid spacing of the model configuration seems to affect the model response to the specific emission reduction case. The median value of the relative potential and absolute potency of NO_x and VOC emission reductions is reported in Table 6 showing the opposing effects on O₃ concentrations with higher impacts on long-term simulations (LT). The order of magnitude in absolute

value of the potency is larger for a NO_x emission reduction compared with a VOC emission reduction.

Models' responses to emission changes: PM₁₀

Applying precursor emission reductions generally leads to a decrease of PM₁₀ concentrations with an absolute potential reduction of -1 to $-11 \mu\text{g m}^{-3}$ if a reduction is applied to ALL precursors together (Fig. 4) during the episodes. Again, the model responses can be very different. For instance, EMEPE and EMEPG have values of -5 and $-11 \mu\text{g m}^{-3}$, respectively, with the same modelling setup but with different emissions, the corresponding relative potentials being approximately -33% and -50% respectively. Looking at individual precursor reductions, NO_x is the emission reduction that displays very different effects between models and cities/regions. For a NO_x emission reduction in AMS012, an increase of concentration is observed for all models while for MAD021, CHIMCIE01M and EMEPG there are contrasting responses. PAR014 and VIE019 have the highest NO_x potencies (Figure S118). For the VOC emission reduction, only WRFZAMG in VIE019 estimates a slight increase of PM₁₀ concentrations (Figure S186). These counter-intuitive effects can be explained by non-linear processes in the chemistry schemes as explained in Clappier et al. (2021) and Thunis et al. (2021a). The highest response to a VOC emission reduction is observed for PAR014 but it remains below -1% in terms of relative potential. For all case studies, the main impact driver is the reduction of PPM with a relative potential in the range -6 to -60% depending on the model and city.

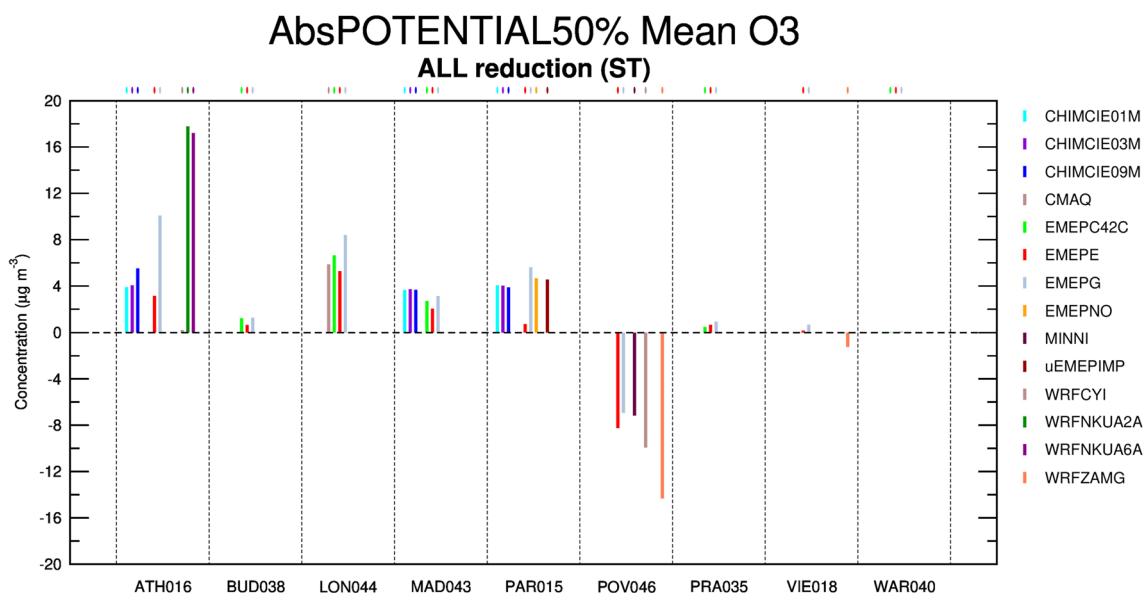


Fig. 3 Absolute potential $APL_{50\%}$ for the mean O₃ values for the short-term episodes with a reduction of 50% for all precursors. At the top of each plot, a small coloured mark is drawn to show that a result

is shown for a given model, to avoid any confusion for low absolute values that cannot be distinguished from the x-axis. Where the value overshoots the scale, the value is written on the plot

Table 6 Median potency (APY) in $\mu\text{g m}^{-3}$ per ton of emissions reduced and relative potential (RPI) in % for the 50% emission reduction for ozone concentrations

Emission precursor	APY ($\mu\text{g m}^{-3} \text{ ton}^{-1}$)		RPI (%)	
	ST episodes	LT simulation	ST episodes	LT simulation
NOx	+0.0239	+0.0648	+2.727	+4.77
VOC	-0.0028	-0.0031	-0.329	-0.846

Using the CHIMERE model in the CHIMLMD configuration, between a resolution of 9km and 3 km for PM_{10} , a difference in the absolute potential for all emission reduction together is observed for the PM_{10} episode over Paris from -7 to $-6 \mu\text{g m}^{-3}$ (Fig. 4). If we focus on PPM emission reductions, the impact drops between -3.5 and $-3 \mu\text{g m}^{-3}$ (Figure S142) showing that the resolution affects species involved in non-linear and linear processes. It is noteworthy that CHIMERE in the different setup of CHIMECIE does not display any differences in emission reductions for the various horizontal resolutions. The impact of the resolution requires a dedicated study to understand this finding. However, it should be borne in mind that the resolution has an impact not only on the resolution of chemical and physical schemes but also on the meteorological fields. Thus, averaging, interpolating or summing meteorological variables over a nested domain onto the corresponding mother domain will not be equal to the value directly calculated in the mother domain, affecting as such further downstream concentration-related results.

For the three EMEP configurations for ST simulations (Fig. 4) at first sight, the emission inventory seems to have a significant impact on the absolute potential particularly over

Lisbon, Prague and Warsaw. This will be analyzed in detail in a follow-up study. Due to the normalization, the relative potential is less impacted by the use of different emissions for LT simulations (Figure S75).

The median relative potential and absolute potency of precursor emission reductions are reported in Table 7. Clearly the effect of VOC emission reductions is the weakest among all precursors, while PPM emission reductions are the most efficient to reduce PM in urban areas. A noteworthy factor of 20 is observed between the absolute potency of NH_3 and NOx emission reductions partly explained by (i) the ratio of the molar masses of these species (ratio of 2.7) which react (on a molar basis) to produce ammonium nitrate, and (ii) the fact that nitrate and nitric acid is in excess over urban areas. Over large domains like Malopolska and Po Valley, the factor is considerably reduced to 10 and even 1 (or less over Po Valley), possibly due to the effect of rural zones included in the domain and higher ammonia emissions, including surroundings under NH_3 -rich regimes. Over a very urbanized area like Paris, this factor reaches 50 emphasizing a general NH_3 limited regime (NO_x -rich regime) over this domain (Petetin et al. 2016). In terms of emission reduction efficiency, it is shown that reducing ammonia over urbanized area is much more efficient to reduce PM than a reduction of NOx.

Indicator of variability

To analyze the variability of responses, an additional indicator—called IND—defined as the root square of the normalized standard deviation of the delta-based indicators previously is computed for each model configuration:

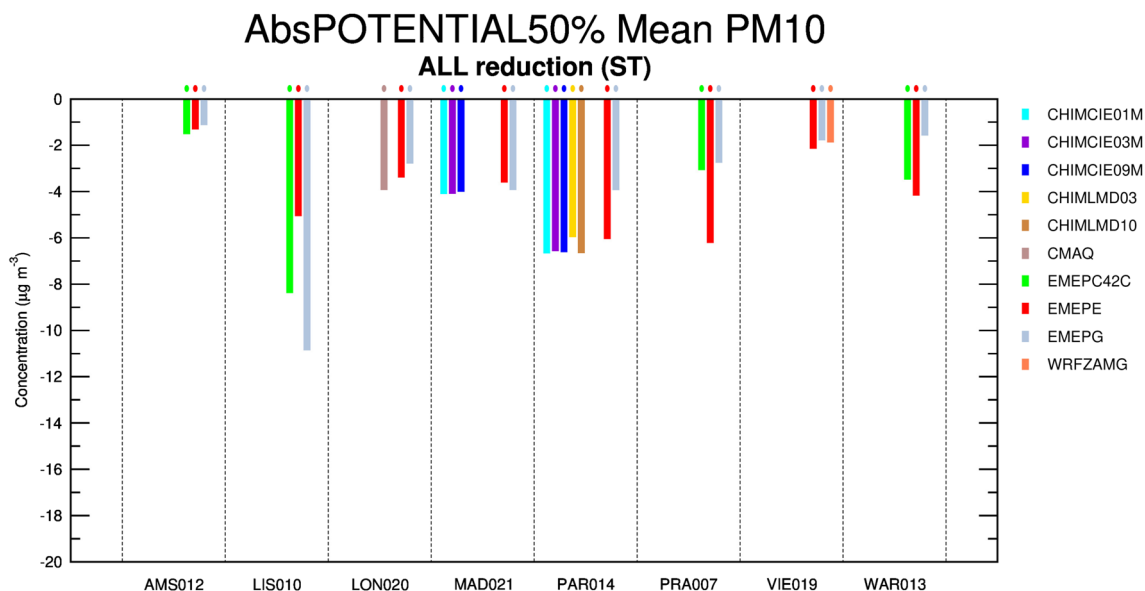


Fig. 4 Absolute potential $APL_{50\%}^{ave}$ for the mean PM_{10} values for the short-term episodes with a reduction of 50% for all precursors. At the top of each plot, a small coloured mark is drawn to show that a result

is provided in the chart for the given model to avoid any confusion for low absolute values that cannot be distinguished from the x-axis. Where the value overshoots the scale, the value is written on the plot

$$VAR_{IND} = \frac{\sqrt{\frac{1}{\Lambda} \sum_{\lambda=1}^{\Lambda} \left(IND_{\lambda} - \frac{1}{\Lambda} \sum_{\lambda=1}^{\Lambda} IND_{\lambda} \right)^2}}{\frac{1}{\Lambda} \sum_{\lambda=1}^{\Lambda} |IND_{\lambda}|} \quad (1)$$

where *IND* is the indicator calculated by Eqs. (9) to (12) of Appendix 3 for each model, where Λ is the number of models providing results. The variability is computed only when at least 3 models are available. We have decided to normalize the variability by the average of the absolute values of indicators. As the normalization of the standard deviation is quite tricky, a possibility would consist of using the range but this method is mostly impacted by outliers (Dodge 2006). Moreover, since indicators can be negative numbers, the use of averaged absolute values avoid the possibility of having mean values close to 0, which would strongly affect the normalization.

The variability of all indicators is synthetized in Fig. 5. The indicators are presented in Appendix 3; the variability of these indicators represent the median of all variabilities computed for a group of cities where at least three models delivered their results.

The indicator of variability is generally higher for responses to emission reductions than for the variability of base case concentrations. It is particularly noteworthy for the ozone episodes (only 6% of variability in base case concentrations) because of the large influence of long-range transport, leaving little impact for the local reductions, as reported in Boleti et al. (2019) and Bossioli et al. (2007) and verified during the COVID-19 pandemic (Cuesta et al. 2022; Menut et al. 2020). However, even if local emission reductions have little effect, they can be very different from model to model leading to a high variability of small values. This finding contradicts the findings of the Citydelta project (Thunis et al. 2007) which reported consistent deltas between models but on a limited number of cities. Even so, in Thunis et al. (2007) and Arunachalam et al. (2006) model, responses were sometimes large for some cities with deltas varying from 1 to 3 ppb for ozone which is a large range but on small absolute values. Also, in the EURODELTA exercise, differences between model

Table 7 Median absolute potency (APY) in $\mu\text{g m}^{-3}$ per ton of emissions reduced and relative potential (RPI) in % for the 50% emission reduction for PM_{10} concentrations

Emission precursor	APY ($\mu\text{g m}^{-3} \text{ton}^{-1}$)		RPI (%)	
	ST episodes	LT simulation	ST episodes	LT simulation
NOx	−0.0006	−0.0017	−0.58	−1.89
VOC	−0.0002	−0.0006	−0.14	−0.53
SOx	−0.0112	−0.0175	−1.92	−3.30
NH3	−0.0359	−0.0279	−3.44	−4.77
PPM	−0.0888	−0.1059	−14.88	−19.52

responses using the potency indicator (Thunis et al. 2010) were large both for ozone and PM_{10} but at a coarse resolution of 50km over Europe.

As shown in Fig. 5, all indicators, the absolute potential, relative potential and absolute potency, show a higher variability for the response (between 20 and 100%) than for emissions and absolute concentrations (between 20 and 50%), particularly in the case of NOx and VOC emission reductions, for both ozone and PM_{10} concentrations.

For PM_{10} episodes, the variability of concentrations exceeds 20% and is often much higher than 100% for the other indicators. In general, the variabilities of the relative potential and absolute potency are lower than for the absolute potential because the respective normalization by concentrations and emissions, respectively, reduce the differences between models. The remaining variability is probably driven by the use of different setups.

The variability for the mean of the highest values (average values above the 95th percentile) is generally higher than for mean values for all PM_{10} concentrations. For ozone, the picture is different since highest values usually occurred in the suburbs or rural places, which are not co-located with ozone precursor emissions.

Regarding the base case, while the variability of PM_{10} concentrations and the precursor emissions has the same order of magnitude (around 20%), for ozone the variability of concentrations (6%) is much lower than the variability of precursor emissions (larger than 50%).

Clearly, NOx and VOC emission reductions induce the highest variability in the indicators for the PM_{10} episodes even if the variability in emissions is, often, the lowest. In general, the reduction of all precursor emissions together gives the lowest variability compared with individual precursor emissions, which is probably due to the compensation of effects. The city-by-city variability does not show a systematic pattern, although, for example, the city of Stockholm shows a very high variability for LT simulations both for ozone and PM_{10} mean concentrations (Figure S213 and S217).

Assessment of linearity and additivity

The 25% and 50% emission reductions are used to calculate a ratio (%) of deviation to linearity (or simply *Linearity*) defined as:

$$Linearity = 100 \times \left(\frac{APL_{50\%,m}}{APL_{25\%,m}} - 1 \right) \quad (2)$$

for each precursor emission precursor (denoted by *m*). Again, a perfect linearity is obtained for an indicator value of 0%. For the linearity, four cases exist with, in some cases, a change of chemical regime that can induce a change of sign of the absolute potential as shown in Table 8. The linearity is defined only for $APL_{25\%,m} \neq 0$.

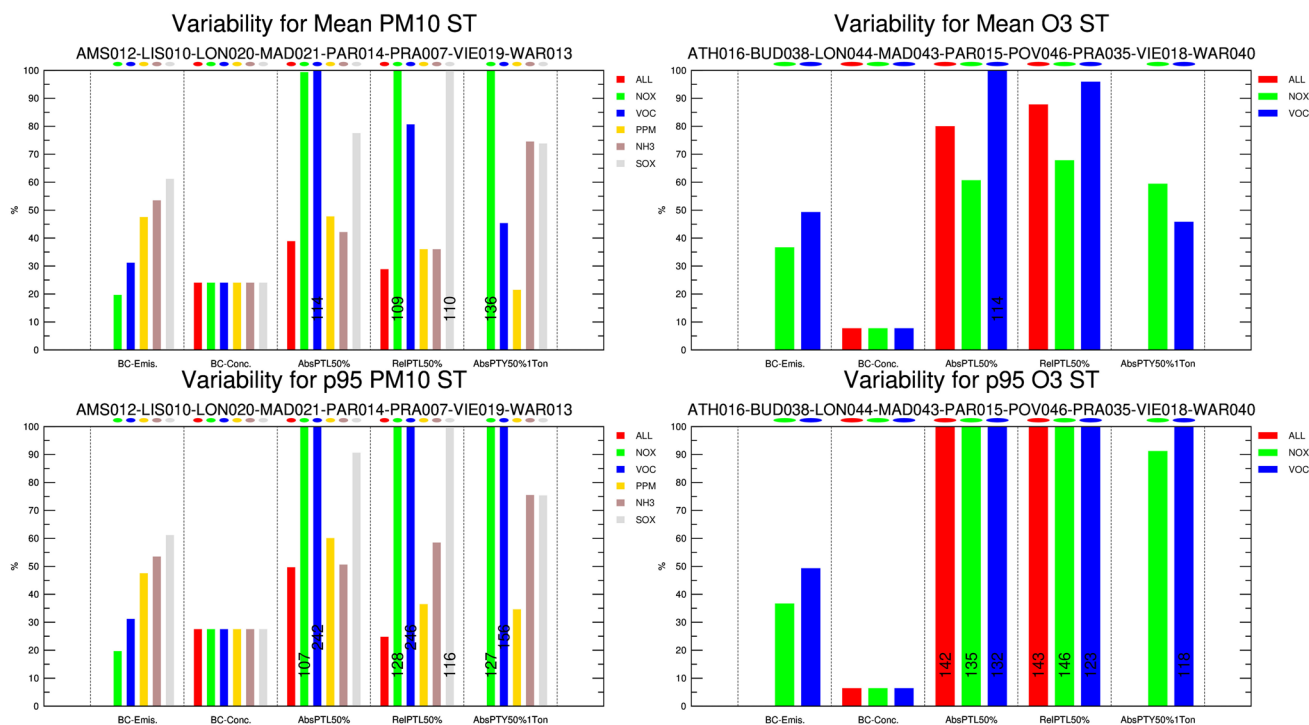


Fig. 5 Variability of model responses calculated as in Eq. (1) for indicators related to the emissions, base case concentrations, absolute potential, relative potential and the absolute potency for the various reductions of precursors for PM₁₀ and O₃ mean and the highest 95th percentiles values (top and bottom panels respectively). At the top of each chart, the list of regions and episodes is provided. The vari-

ability is also provided for the average concentrations and emissions over the target domain of emission reductions. The variability is an average value computed for the group of cities (episodes) mentioned at the top of each chart, computed only when the results of at least 3 models were available

The available scenarios also allow the analysis of the additivity property, by comparing the sum of emission reductions (50%) applied separately called “ADD” ($\sum_m APL_{50\%,m}$) with the combined reduction of precursor emissions called “ALL”. Here, we test this property on the absolute potential. To do so, the following criteria called “deviation to additivity” in % (or simply *Additivity*) is defined as:

$$Additivity = 100 \times \left(\frac{APL_{50\%,ALL}}{\sum_m APL_{50\%,m}} - 1 \right) \quad (3)$$

If the model is perfectly additive, this indicator value is 0%. The additivity coefficient is defined only for $\sum_m APL_{50\%,m} \neq 0$ and the different cases are identified in Table 9.

Note that the linearity and additivity indicators are very sensitive to the value of the denominator and can overshoot in some cases for very low values of absolute potential.

The results for the deviation to linearity when reducing all precursor emissions are shown in Fig. 6 for ozone and in Fig. 7 for PM₁₀. While for PM₁₀ there is a quasi-linearity (deviation to linearity between 0 and 5%) mainly driven by the perfect linearity when applying an emission reduction of PPM, the picture is totally different for the response regarding ozone concentrations (Fig. 6 and Fig. 7). Except in London,

Madrid and Paris, and to a lesser extent over Prague and the Po Valley, in cities like Vienna and Warsaw, the models show a negative deviation to linearity often larger than -50% . In Warsaw, a value of -143% is computed for EMEPE meaning that the sign of the response of O₃ changes with the strength of the emission reduction. This is due to the change of regime when applying a stronger emission reduction, switching from a VOC- to a NO_x-limited regime. Interestingly, applying separate emission reductions to NH₃ or NO_x emissions show that from a 25 to a 50% reduction, we obtain an increase of the potential reduction of PM₁₀ mean concentrations for long-term simulations (Figures S89 and S111). This clearly shows the change of chemical regime upon precursor availability and aerosol thermodynamics. Indeed, the species primarily impacted by the emission reduction reaches on average a tipping point becoming limiting and then enhancing the efficiency of the reductions. The importance of ammonia emission reductions to limit air pollution have already been highlighted in Europe (Bessagnet et al. 2014a, b) particularly when applied over large domains. NH₃ is considered in excess in most of Europe. However, for the values exceeding the 95th percentile in Madrid (MAD004), the picture is rather different, where a 50% emission reduction of NO_x looks less efficient to reduce peak PM₁₀ concentrations (Figure S112).

The case of Paris for an emission reduction of SO_x is noteworthy (Figure S166). while for CHIMERE in configuration CHIMCIE a quasi-linearity is observed independent of the horizontal resolution. CHIMERE in the CHIMLMD configuration has a reduction of efficiency for PM₁₀ concentrations that decreases from emission reductions of 25 to 50% and a strong dependence on horizontal resolution. However, for the CHIMLMD configuration, the absolute impact on concentrations is very low. Regarding the impact of reducing NO_x, a similar behaviour between CHIMCIE and CHIMLMD is observed with an amplified potential reduction of PM₁₀ concentrations and higher absolute impacts on PM₁₀

(up to $-0.7 \mu\text{g m}^{-3}$). At this stage of the analysis, it is not possible to explain the reason for these behaviours and identify which part of the configuration plays the most important role in explaining the differences: the model version/type, the emission dataset or the non-linear processes involved in the secondary PM chemistry. This behaviour might be a result of the calculation of statistical ratios on very low absolute values, leading to a change of sign, or it can derive from formation subprocesses, affected by the concentrations of gaseous precursors, such as the formation of ammonium nitrate and sulphate inorganic species. For example, the neutralization of ammonia by nitric acid (formed by NO_x oxidation) competes with the

Table 8 The four cases of linearity

Cases		Meaning
Linearity > 0	$ APL_{50\%,m} > APL_{25\%,m} $ with $\text{sign}APL_{50\%,m}^{\text{ave}} = \text{sign}APL_{25\%,m}^{\text{ave}}$	The decrease or increase is amplified from 25 to 50% reduction
Linearity = 0	$APL_{50\%,m} = APL_{25\%,m}$	The 25% and 50% related increases or decreases are equal
$-100\% < \text{Linearity} < 0$	$ APL_{50\%,m} < APL_{25\%,m} $ with $\text{sign}APL_{50\%,m} = \text{sign}APL_{25\%,m}$	The decrease or increase is reduced from 25 to 50% reduction
Linearity < -100%	$\text{sign}APL_{50\%,m} \neq \text{sign}APL_{25\%,m}$	The sign of impact changes from 25 to a 50% reduction

Table 9 The four cases of additivity (ALL and ADD are respectively reductions with all precursors together, and the sum of individual precursor emission reductions)

Cases		Meaning
Additivity > 0	$ APL_{50\%,\text{ALL}} > \sum_m APL_{50\%,m} $ with $\text{sign}APL_{50\%,\text{ALL}} = \text{sign}\sum_m APL_{50\%,m}$	The decrease or increase is amplified from ADD to ALL reduction
Additivity = 0	$APL_{50\%,\text{ALL}} = \sum_m APL_{50\%,m}$	Increases or decreases are equal
$-100\% < \text{Additivity} < 0$	$ APL_{50\%,\text{ALL}} < \sum_m APL_{50\%,m} $ with $\text{sign}APL_{50\%,\text{ALL}} = \text{sign}\sum_m APL_{50\%,m}$	The decrease or increase is reduced from ADD to ALL reduction
Additivity < -100%	$\text{sign}APL_{50\%,\text{ALL}} \neq \text{sign}\sum_m APL_{50\%,m}$	The sign of impact change from ADD to ALL reduction

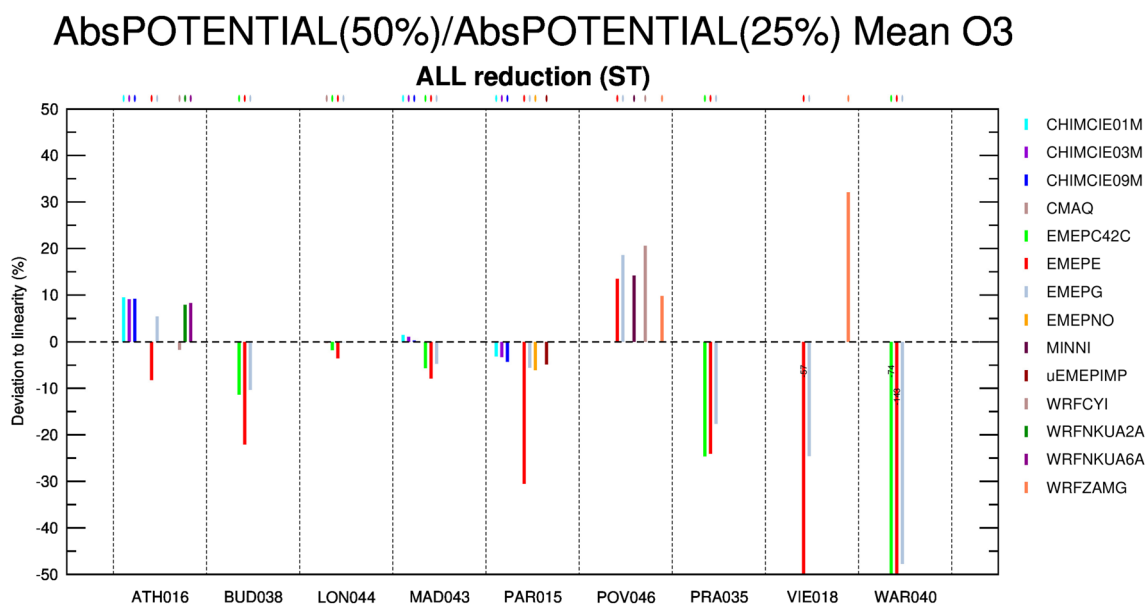


Fig. 6 Deviation to linearity (%) for ozone for the ST simulations applying ALL (NO_x, VOC) emission reductions

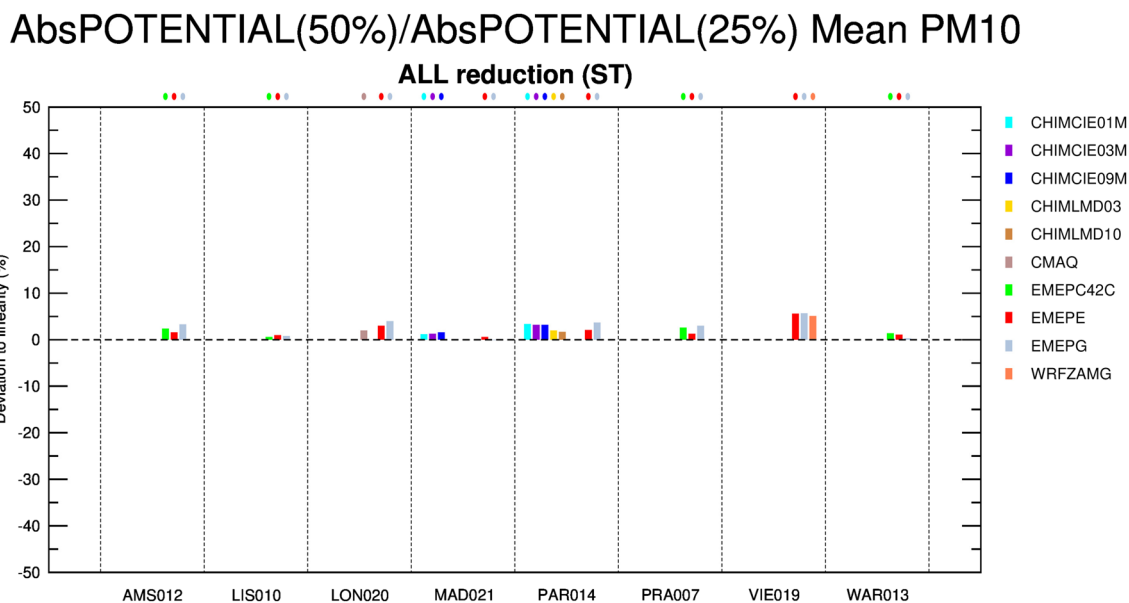


Fig. 7 Deviation to linearity (%) for PM₁₀ for the ST simulations applying ALL (NO_x, VOC, NH₃, SO_x, PPM) emission reductions

formation of the more thermodynamically stable ammonium sulphate, in which ammonia gas neutralizes the sulfuric acid aerosols in the atmosphere (Kushta et al. 2021). Any perturbation might accelerate and/or reduce the efficiency of the formation depending on the reduction combination (sole species or combination).

Regarding the additivity of separate reduction of 50%, the results also differ between O₃ and PM₁₀ for ST simulations. For PM₁₀, the contributions are rather additive with a deviation below 15% (Fig. 8), and often

positive, showing a benefit when various pollutant emissions are reduced at the same time. It is noticeable that the WRFZAMG configuration increases the concentration reductions by 50% when applying all emission reductions together in Vienna. This behaviour requires further analysis since WRF-Chem is used with feedbacks on the meteorology that in turn affects the concentrations. For ozone, additivity is clearly not the rule as shown in Fig. 9 for short-term episode and also in the Po Valley for the long-term simulation

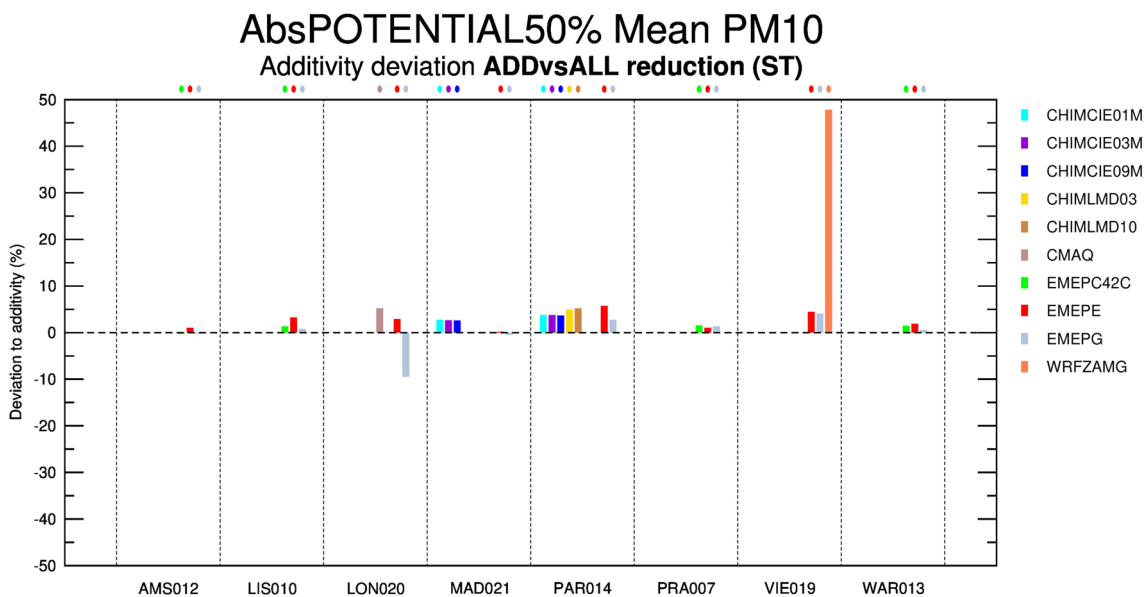


Fig. 8 Deviation to additivity (%) for PM₁₀ for the ST simulations applying ALL (NO_x, VOC, NH₃, SO_x, PPM) versus adding all contributions (ALL = NO_x + VOC + NH₃ + SO_x + PPM) emission reductions (– 50%) for the absolute potential

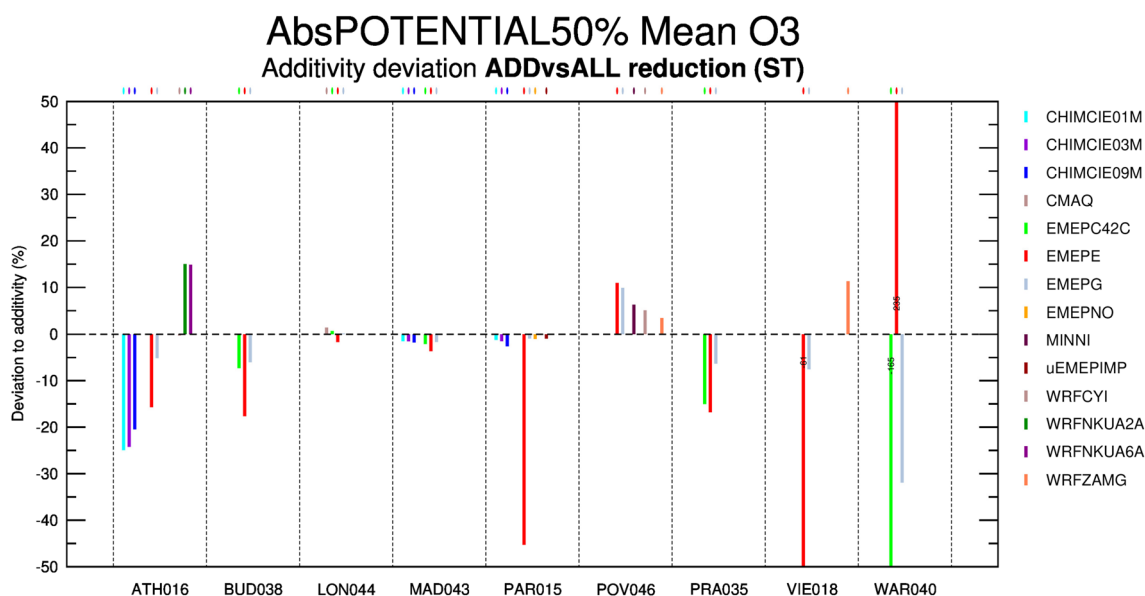


Fig. 9 Deviation to additivity (%) for O_3 for the ST simulations applying ALL (NO_x, VOC) versus adding all separate contributions (ADD=NO_x + VOC) emission reductions (–50%) for the absolute potential

and especially for the highest concentrations in the LT simulations (Figure S2). However, for some cities like London, Madrid and Paris, most of the configurations show a rather additive behaviour. When analyzing the difference in terms of impact between the combined NO_x and VOC reductions and the sum of individual reduction impacts (Figures S2, S4), the lowest deviations were found for the Brussels and Madrid cases, with a full additivity in the EMEPC2, EMEPCE and RIOCHIRC setups. For the Warsaw case (WAR040) as the absolute potential is very low (Fig. 3) in absolute values, the deviation to linearity is very important and clearly shows the limitation of studying such indicators with low absolute values.

Conclusions and perspectives

This study presents a comprehensive application of the FAIRMODE platform (<https://fairmode.jrc.ec.europa.eu>) for evaluating the variability of the responses of different air quality models' applications to prescribed emission reductions over various European cities and two highly polluted areas (Po Valley and Malopolska). Based on standard deviation calculation, using model outputs, we have analyzed the variability of several indicators such as APL and APY. The main results can be summarized as follows:

- Air quality models' applications show significant differences (variability, as defined in this study, often exceeds 20%) in the concentration changes (deltas) for the 25 and 50% emission reductions d ;
- The variability of model responses using delta-based indicators is higher for PM₁₀ than for O_3 ;
- The variability of model responses to emission reductions is higher than the variability of modelled base case concentrations and of emissions used as input;
- Relative indicators like the relative potential (normalized by the concentration) and the absolute potency (normalized by the emission reductions) have a lower variability compared with the absolute potential (which is proportional to the delta of concentrations);
- For O_3 , the analysis of linearity and additivity of model responses show a clear impact of non-linear chemistry processes that leads to a large deviation to linearity and additivity of concentrations in relation to emission reductions;
- For PM, the response is, in general, more linear and additive, particularly, as expected, when reducing the primary emissions of particles which weakly perturb the chemical and physical processes involved in the PM formation;
- One should be cautious in the interpretation of these indicators because they are built on averages and ratios of values that can be very low and with different signs. More work should be devoted to develop new ones.

This type of exercise may give indications regarding the limits of the efficiency of mitigation measures. Modelling results show that applying emission reductions on several sectors (often related to a main precursor) at the same time seems more beneficial for reducing PM concentrations than reductions of individual precursors.

The lower variability between models due to a normalization by concentrations or emissions reduces the influences of different input data and permits the evaluation of the role of other processes that can explain the variability of concentration deltas. As future work, several additional analyses are planned to disentangle the role of individual

processes, differences in setup and input data that give rise to the variability between model responses. The role of emissions, chemistry schemes, meteorology, online/offline coupling strategies and horizontal resolution will be of particular interest to modellers to improve the application of their models for assessing mitigation strategies aimed at improving air quality in cities and regions.

This platform and its application is an ongoing programme of work to assess the behaviour of models when applying emission reduction scenarios and test the robustness of their application to evaluate mitigation strategies to curb air pollution.

Appendix 1. Definition of target domains

Please see Table 10.

Table 10 List of selected domains defined by 4 corners in longitude and latitude (regional domains are specified in italics)

Country	City or region	Lon. Min (°E)	Lon. Max (°E)	Lat. Min (°N)	Lat. Max (°N)	Greater City area (km ²)
Austria	Vienna	15.87	16.87	47.70	48.70	9205
Belgium	Brussels	4.05	4.65	50.55	51.15	3266
Bulgaria	Sofia	22.92	23.72	42.30	43.10	5717
Croatia	Zagreb	15.63	16.33	45.46	46.16	5059
Czech Republic	Prague	14.04	14.84	49.68	50.48	6980
Denmark	Copenhagen	12.32	12.82	55.43	55.93	2800
Estonia	Tallinn	24.40	25.10	59.08	59.78	4340
Finland	Helsinki	24.60	25.20	59.87	60.47	3822
France	Paris	1.80	2.90	48.30	49.40	12,098
Germany	Berlin	12.76	14.06	51.87	53.17	17,484
Greece	Athens	23.43	24.03	37.68	38.28	3030
Hungary	Budapest	18.64	19.44	47.09	47.89	6393
Ireland	Dublin	−6.65	−5.85	52.95	53.75	6991
Italy	Rome	12.09	12.89	41.50	42.30	5744
Latvia	Riga	24.00	24.20	56.85	57.05	304
Lithuania	Vilnius	24.93	25.63	54.33	55.03	4247
Luxembourg	Luxembourg	5.88	6.38	49.36	49.86	2596
Netherlands	Amsterdam	4.60	5.20	52.07	52.67	2915
Norway	Oslo	10.30	11.20	59.47	60.37	7428
Poland	Warsaw	20.51	21.51	51.73	52.73	8615
Portugal	Lisbon	−9.43	−8.83	38.42	39.02	3901
Romania	Bucharest	25.90	26.30	44.23	44.63	1066
Slovakia	Bratislava	16.86	17.36	47.89	48.39	2052
Slovenia	Ljubljana	14.25	14.75	45.81	46.31	2556
Spain	Madrid	−4.15	−3.25	39.96	40.86	6825
Sweden	Stockholm	17.62	18.52	58.88	59.78	7093
UK	London	−0.63	0.37	51.00	52.00	8024
Poland	Malopolska	18.00	23.00	48.70	51.50	-
Italy	Po Valley	6.50	14.00	43.50	47.00	-

Appendix 2. Full description and key features of models

EMEP operated by JRC/METCLIM

The EMEP model (Simpson et al. 2012) domain stretches from 15.05° W to 36.95° E longitude and 30.05° N to 71.45° N latitude with a horizontal resolution of 0.1° × 0.1° and 20 vertical levels, with the first level around 50m. The model uses meteorological initial conditions and lateral boundary conditions from the European Centre for Medium-range Weather Forecasting (ECMWF IFS) for the meteorological year 2015 (Owens and Hewson 2018). The temporal resolution of the meteorological input data is daily, with 3-h time steps. The meteorological fields for EMEP are retrieved on a 0.1° × 0.1° longitude-latitude coordinate projection. Vertically, the fields on 60 eta (η) levels from the IFS model are interpolated onto the 37 EMEP sigma (σ) levels. The MARS equilibrium module is used to calculate the partitioning between gas and fine-mode aerosol phase for inorganic species sulphate/nitrate/ammonium (Binkowski and Shankar 1995). More information on the gas and aerosol partitioning, meteorological drivers, land cover, model physics and chemistry are given in Simpson et al. (2012). The model was operated over Europe, for which we have four different emission inventories available. The following emission datasets are used for EMEPE, EMEPG, EMEPC2 and EMEPC42C configurations, respectively: Edgar 5.0 (Crippa et al. 2018; Janssens-Maenhout et al. 2019; Oreggioni et al. 2021), EMEP (Mareckova et al. 2019), CAMS version 2.2.1 and CAMS version 4.2 including condensables (Granier et al. 2019; Kuenen et al. 2022).

WRF-Chem operated by CYI

The WRF-CYI model is configured using the Weather Research and Forecasting model with Chemistry (WRF-Chem) version 3.9.1.1 (Skamarock et al. 2008) to perform simulations of meteorological and air quality conditions for O₃ episodes in Athens and Po Valley. For each episode, two nested domains are used with the parent domain covering south-eastern Europe at 20 km (Athens) and 30 km (Po Valley) grid spacing while the nested domain is focused on the respective area of interest with a horizontal resolution of 10 km. The configuration of the physical and chemical processes follows that of Georgiou et al. (2018) with the following differences highlighted in Table 5. Emissions are taken from EDGAR v5 database (Crippa et al. 2018) that includes annual emission fluxes (with monthly temporal variation) of the main gaseous and aerosol pollutants (SO₂, CO, NO_x, CO, BC, OC, VOC and PM_{2.5} primary

emissions) while natural emissions of sea salt aerosols and biogenic volatile species are generated online using weather and land use data as described in Georgiou et al. (2018). The meteorological data are derived from the Global Forecast system (GFS) datasets at 0.5° × 0.5° and updated every 6 h (NCEP 2015). Boundary conditions are taken from Emmons et al. (2010), the gas phase chemistry is RADM2 (Stockwell et al. 1990) and the aerosol module is MADE/SORGAM (Ackermann et al. 1998; Schell et al. 2001). The cloud physics scheme is the Morrison double moment (Morrison et al. 2005), the cumulus parameterization is Grell 3D (Grell and Dévényi 2002) and the land surface physics is the Noah land surface model (Chen and Dudhia 2001) with the RRTMG scheme for the Longwave & Shortwave radiation (Mlawer et al. 1997) and the Yonsei University Planetary Boundary layer (Hong et al. 2006).

WRF-Chem operated by NKUA

The WRFNKUA model is based on the Weather Research and Forecasting (WRF) model, Version 4.2, fully coupled with chemistry. WRF-Chem simulations account for both the direct and indirect effect of aerosols (Grell et al. 2005). Four domains with a horizontal resolutions of 55.5 km, 18.5 km, 6 km and 2 km, respectively, are used, where the three inner domains are all two-way nested to their parent domain. Athens is the innermost domain. The last two domains (named WRFNKUA6A and WRFNKUA2A) are used in this study. The Lat/Long projection is used. In the vertical, 40 terrain-following sigma levels, with the lowest model level at about 14 m. The RRTMG scheme for the Longwave & Shortwave radiation (Iacono et al. 2008) and the Yonsei University Planetary Boundary layer parameterization (Hong et al. 2006) is used. The Morrison double moment scheme for cloud physics (Morrison et al. 2005) and the cumulus parameterization Grell 3D (Grell and Dévényi 2002) are also implemented. The gas phase chemistry is RADM2 (Stockwell et al. 1990, 1997), and the aerosol module is MADE/SORGAM (Ackermann et al. 1998; Schell et al. 2001). The EDGAR-HTAP (Emissions Database for Global Atmospheric Research-Hemispheric Transport of Air Pollution) global emission inventory is used including shipping with a horizontal grid resolution of 0.1° × 0.1° (Janssens-Maenhout et al. 2015) and a reference year of 2010. Biogenic emissions are calculated online with the MEGAN module (Guenther et al. 2006) while the initial and boundary conditions for gases and aerosols come from simulation of CAM-chem in CESM2.0 (Emmons et al. 2020). For the other physical parameterizations and information on natural and fire emissions, the reader is referred to the setup of Bossioli et al. (2021).

WRF-Chem operated by GeoSphere Austria

The WRF-Chem version 3.9.1.1 (Grell et al. 2005) simulations were conducted on a European domain (12×12 km) and a nested domain covering Central Europe (4×4 km). The results of the nested domain were used for the study. RADM2 (Stockwell et al. 1990) chemical mechanism and MADE/SORGAM (Schell et al. 2001) aerosols (*chem_opt* = 2) together with the following physics options were applied for the simulations: Rapid Radiative Transfer Method for Global (RRTMG) long-wave and short-wave radiation scheme (Iacono et al. 2008), MYNN2 Planet Boundary Layer (PBL) scheme (Nakanishi and Niino 2006), NOAH land surface model (Campbell et al. 2019) and the Grell three-dimensional (3D) ensemble cumulus parameterization (Grell and Freitas 2014). Beside the anthropogenic emissions (Kuenen et al. 2014), the model includes biogenic emissions calculated by MEGAN (Guenther et al. 2006) and dust (LeGrand et al. 2019) and sea salt emissions from the Goddard Chemistry Aerosol Radiation and Transport model as GOCART (Chin et al. 2002).

EMEP operated by Met Norway

For the EMEPNO configuration, the EMEP MSC-W chemistry-transport model (Simpson et al. 2012) is used (version rv4.42) at a 0.1° resolution, for a domain covering the area $30\text{--}82^\circ\text{N}$, $30^\circ\text{W}\text{--}90^\circ\text{E}$. Meteorological fields are taken from the IFS model (ECMWF IFS cy40r1) at a 0.1° resolution. The official EMEP emission inventory for 2015 as reported in 2019 was used Mareckova et al. (2019). The EMEP model also outputs local fractions for running the uEMEP model.

uEMEP is a downscaling model built on the EMEP setup to obtain concentration maps at a higher resolution of 250 m by recalculating contributions from local emission sources as Gaussian plumes (Denby et al. 2020; Mu et al. 2022). First, emissions for three GNFR (Gridding Nomenclature for Reporting) sectors are downscaled to 250 m resolution using proxy data with details given in Mu et al. (2022): population and building density data for GNFR C (residential combustion), OpenStreetMap (<https://planet.osm.org/>) for GNFR F (road transport) and AIS data of ship positions for GNFR G (shipping). Then, for each hour at each $250\text{ m} \times 250\text{ m}$ grid cell within the defined city boundary, the contributions to concentrations at that cell from all emission sources of the three sectors within a surrounding domain of size $0.3^\circ \times 0.3^\circ$ (longitude-latitude) are recalculated through Gaussian plumes. The local fraction information from the EMEP model is used to remove the contributions from these downscaled sources

from the original EMEP concentrations, thus avoiding double counting as detailed in Denby et al. (2020). Only the NO_x emissions and primary PM emissions are downscaled, and the only chemical reaction accounted for in the Gaussian plumes is the NO_x–O₃ interaction, using the Düring approach (Düring et al. 2011; Maiheu et al. 2017). For annual mean runs, the downscaling is performed directly on the annual mean concentrations, using a rotationally symmetric dispersion kernel (Denby et al. 2020). A similar setup using EMEP + uEMEP was applied in Mu et al. (2022) for calculating high-resolution concentration maps for all of Europe.

The distinction between the setups of uEMEPIMP and uEMEPTAG is in how emission reduction scenarios are calculated. They both use the same base case simulation, but while uEMEPIMP uses the standard brute-force method of rerunning EMEP + uEMEP for each reduction scenario using reduced emissions, uEMEPTAG calculates the scenarios without rerunning the model. Instead, reductions in concentrations are deduced from the tagging of primary PM and NO_x emitted within the city boundaries in the base case simulation. New NO₂ and O₃ concentrations are calculated by reapplying the Düring scheme with the reduced NO_x concentrations. This setup is therefore limited to the reduction scenarios of NO_x and PPM and its results do not include any effects on secondary particle formation.

LOTOS-EUROS and ADMS operated by DHMZ

LOTOS-EUROS (Manders et al. 2017) is an open-source chemical transport model that was used to assess the impact of emission reduction over Zagreb (Croatia). The model used two domains. The outer domain encompassed an area from -10°W to 45°E longitude and 30°N to 60°N latitude with a horizontal resolution of $0.5^\circ \times 0.25^\circ$. The nested domain encompassed an area from 15.63 to 16.33°E longitude and 45.46 to 46.16°N with a horizontal resolution of $0.1^\circ \times 0.05^\circ$. For vertical resolution, 5 layer mixing scheme was used with a surface layer fixed at 25 m in height, a dynamic layer that extends from the top of the surface layer to the top of the mixing layer and three more dynamic reservoir layers on top that reach up to 5 km in height. An identical meteorological driver, taken from ECMWF IFS (Owens and Hewson 2018) (F1280 grid), was used for both domains. For consistency, both domains used the same emission dataset prepared using the CAMS-REG-AP v2.2.1 as a base, with an appropriate reduction of emissions only within the nested domain.

ADMS-Urban (Carruthers et al. 1994; Hood et al. 2018), Version 4.1.1., is a quasi-Gaussian plume air dispersion model, the most comprehensive version of the Atmospheric Dispersion Modelling System (ADMS). The model was set

up for the Zagreb agglomeration and the year 2015. Chemistry schemes involving NO_x, NO₂ and ozone were implemented. The dispersion calculations are driven by hourly meteorological data obtained from Zagreb-Maksimir meteorological site and are taken to be representative of the whole domain. The model uses background data from the Desinić rural-background site (hourly sequential air quality data that represents the contribution of regional transboundary pollution), and emissions at a 500 m × 500 m resolution were obtained from the Croatian National Emission Inventory (source: Ministry of Economy and Sustainable Development). Two large point sources were explicitly modelled.

WRF-CHIMEREv2020r1 operated by LMD

The CHIMERE model is a regional chemistry-transport model that can be used in both online and offline configurations in its latest version (Mailler et al. 2017; Menut et al. 2021) for research, future scenarios and operational forecast purposes (Bessagnet et al. 2020; Lapere et al. 2021; Menut et al. 2020). For online modelling, it is coupled with the WRF (Weather Research Forecast) meteorological model (Skamarock et al. 2008). The model needs a set of gridded data as mandatory input: emission data for both biogenic and anthropogenic sources, land use parameters, boundary and limit conditions, and other optional inputs such as dust and fire emissions. Given these inputs, the model calculates the concentrations and wet/dry deposition fluxes for a list of gaseous and aerosol species (depending on the chosen chemical mechanism).

In this study, the model was coupled with WRF using the NCEP input data (NCEP 2015) for the global meteorological conditions. It was run on a triple nested configuration, with a coarse domain covering the whole of Europe at a 30 km × 30 km resolution (164 × 165 cells), the intermediate domain with a 10 km × 10 km resolution (45 × 45 cells), while the finest domain focused on the Paris region with a 3 km × 3 km resolution (51 × 52 cells). The vertical resolution contains 15 layers starting from the surface going up to 300 hPa. No fire emissions were used. Boundary conditions were taken from CAMS 3-hourly reanalysis global runs. All major aerosol groups are activated including elemental carbon, sulphate, nitrate, ammonium, SOA, dust, salt and PPM, taking into account coagulation, nucleation and condensation processes over 10 size bins ranging between 10 nm – 40 μm. Anthropogenic emissions were prepared using the CAMS regional inventory (Granier et al. 2019) for both reference simulations and reduction scenarios.

WRF-CMAQ operated by UH-CACP

The Community Multi Scale Air Quality Modelling System (CMAQ) is a prognostic air quality suit of models developed by the U.S Environmental Protection Agency (USEPA). The model is based on the concept “one atmosphere” and accounts for complex interactions among several pollutants but also complex process interaction between regional and urban scales. CMAQ includes a Meteorology Chemistry Interface Processor (MCIP) (Otte et al. 2005), an Initial Condition (ICON) processor, a Boundary Condition (BCON) processor and the chemistry transport model (CTM) (US EPA Office of Research and Development 2020; Xu and Chen 2021). The chemistry transport model is used to simulate aerosol and gas chemistry in addition to the transport and deposition of chemical species while modelling atmospheric processes. CMAQ is incapable of independently calculating the complex meteorological processes essential for air quality modelling and requires Weather Research and Forecast (WRF) model output to produce the meteorological fields. Furthermore, CMAQ requires its emission data to be pre-processed in specific format. This can be computed using the Sparse Matrix Operator Kernel Emissions (SMOKE) and Model of Emissions of Gases and Aerosols from Nature (MEGAN) (Guenther et al. 2006).

In this study, the numerical and emissions processing models WRF (version 4.2), CMAQ (version 5.3.2) (Campbell et al. 2019; US EPA Office of Research and Development 2020), SMOKE version 4.6 (Baek and Seppanen 2018) and MEGAN version 2.0.4 (Guenther et al. 2006) were used to simulate the spatial and temporal distribution of air pollutant concentrations for ozone, PM_{2.5}, PM₁₀, NH₃, NO_x and VOC. The meteorological fields were generated using initial and boundary conditions from the NCEP GFS dataset with temporal and spatial resolutions of 0.25° and a 3-h time step to drive WRF (NCEP 2015). Three domains were used: the outer domain (spatial resolution 25 km × 25 km), middle domain (5 km × 5 km) and inner domain (1 km × 1 km). The same domains were also used for CMAQ. The anthropogenic emissions used for the simulation were UK National Emissions Inventory (2015; 1 km × 1 km) merged with Edgar v5 2015 inventory for missing values. The NAEI inventory consists of eleven SNAP sectors (Kuenen and Trozi 2019; Ntziachristos and Boulter 2019): Nature, Extraction distribution of fossil fuels, Agriculture, Industrial combustion, Industrial processes, Other mobile sources, Power generation, Residential commercial and other combustions, Road transport, Solvent use, Waste treatment and disposal. The main pollutants are carbon dioxide (CO), sulphur dioxide (SO₂), non-methane volatile organic compounds (NMVOC), particulate matter (PM_{2.5} and PM₁₀), nitric oxides (NO_x) and

methane (CH₄). Due to the emissions inventory being annual totals and CMAQ requiring emission input as mass flow rates per area, temporal profiles were applied to the annual values. The profiles used are those of TNO (Bultjes et al. 2003). In addition, the biogenic emissions were estimated in MEGAN using meteorological and land use/land cover parameters as input data. The dust and sea salt emissions were calculated inline of the CMAQ CTM model. Initial and Boundary condition driver data for the CTM model were provided by The Community Atmosphere Model with Chemistry (CAM-chem)(Tilmes et al. 2019).

IFS-CHIMEREv2017r4 operated by CIEMAT

The CHIMERE chemistry transport model v2017 (Mailler et al. 2017) was used to evaluate the impacts of the emission reductions. This model has been extensively used in Europe and in particular in Spain (Brands et al. 2020; Vivanco et al. 2008, 2009). Four domains were considered for the simulations centred on Madrid, Athens and Paris with horizontal resolutions of 0.27°, 0.09°, 0.03° and 0.01° (respectively named as CHIMCIE27M, CHIMCIE09M, CHIMCIE03M, CHIMCIE01M). The model was run with MELCHIOR2 chemical mechanism. Emissions were obtained from the EMEP database a 0.1° × 0.1° grid resolution (Mareckova et al. 2019). For the Spanish domains, the national emission inventory for Spain was used on the same grid as the EMEP emissions for the Spanish grid squares. The meteorological fields were adapted from simulations by the European Centre for Medium-Range Weather Forecasts, ECMWF (www.ecmwf.int); the Integrated Forecasting System (IFS) for 2015, obtained from the MARS archive at ECMWF through the access provided by AEMET for research projects. Boundary conditions for the coarsest resolution domains were taken from LMZ-INCA and GOCART climatological simulations.

MINNI operated by ENEA

The air quality modelling system MINNI (Mircea et al. 2014, 2016) is composed of the meteorological model WRF v3.9.1.1 (Skamarock et al. 2008), the anthropogenic emission processor EMMA, the meteorological processor SURFPRO (ARIANET 2011) and the chemical transport model FARM the Flexible Air Quality Regional Model (Silibello et al. 2008). FARM was configured with SAPRC-99 gas phase mechanism (Carter 2000), AERO3 dynamic aerosol model (Binkowski and Roselle 2003) based on three interacting lognormal distributions representing the main processes (nucleation, coagulation and growth), secondary inorganic model ISORROPIA (Nenes et al. 1998) and secondary organic model SORGAM

(Schell et al. 2001). Dry deposition was simulated using a resistance model (Wesely 1989) and the biogenic emissions were calculated with the MEGAN v2.04 model (Guenther et al. 2006).

The simulations were carried out over the Po Valley domain with a horizontal spatial resolution of 4 km. The national emission inventory distributed by ISPRA (Italian Institute for Environmental Protection and Research) was used with provincial level (NUTS3) detail and boundary conditions from the simulation at national level described in (Vitali et al. 2019). The FARM simulation has been done with 16 fixed vertical layers terrain-following and the depth of first layer is 40 m.

CHIMERE + RIO operated by IRCLENE

Air quality projections were calculated in two steps, thanks to a methodology developed by the research organization VITO. The first step is achieved by calculating the reference scenario and the scenarios with emission reductions in Brussels thanks using the CHIMERE CTM model v2017 (Mailler et al. 2017). A run configuration of two nested domains with meteorological ECMWF data for 2015 was used. The parent domain at a 0.5° × 0.5° resolution covers the whole European zone, and the nested domain at 0.1° × 0.1° covers North-Western Europe, centred on Belgium. The emission dataset includes point and surface emissions, and bottom-up emissions were used within Belgium and top-down emissions were used outside Belgium. Emission reductions over Brussels were applied only in the nested domain.

As a second step, a tendency was carried out for each 0.1° × 0.1° grid cell by calculating a regression of the CTM daily concentrations between the base case and the scenario cases. These trends were applied to a best estimate of the concentrations of the base case to determine the scenario concentrations. This best estimate was achieved by an intelligent interpolation of the observed concentrations via the RIO interpolation method (Janssen et al. 2008), resulting in higher resolution (4 × 4 km) concentrations, and so the results were also downscaled using this procedure. The application of trends of RIO reference concentrations rather than the absolute or relative differences for calculating air quality projections is an alternative approach of calibration that accounts for changes in CTM bias.

Appendix 3. Detailed description of indicators

The following notation will be used for the definition of indicators. Capital letters are used for the aggregated values (sum of emissions or averaged values) over the area A_k where precursors are reduced, and lower case for individual grid cell with coordinates (i, j) or (i, j, t) , if we consider time.

<p>k Zone of emission reductions as defined in Table 1</p> <p>m Emission precursor name (NO_x, VOC, PPM, SO_x or NH₃) or all together</p> <p>n Pollutant name, such as O₃, PM₁₀ and NO₂</p> <p>α Percentage emission reduction for the scenarios (50% or 25% here)</p> <p>s Simulation scenario denoted as 50%NO_x, etc. ... or base case (BC) referring to the level of reduction and the precursor involved</p> <p>i, j Grid cell coordinate respectively in longitude and latitude</p> <p>I, J Total number of longitude and latitude coordinates</p> <p>t Current time in hours</p> <p>T Total number of recorded hours of the simulation</p>	<p>$e_{ij}^{m,k,s}$ Emission of precursor m over zone k for grid cell $(i, j) \in A_k$ for simulation s</p> <p>$c_{ij,t}^{n,k,s}$ Concentration of pollutant n over zone k for grid cell $(i, j) \in A_k$ for simulation s at time t</p> <p>$E_{Total}^{m,k,s}$ Total emission of precursor m over zone k for simulation s</p> <p>$C_{Mean}^{n,k,s}$ Averaged concentration of pollutant n over zone k for simulation s</p>	<p>The analysis was performed for two types of averaging over the emission reduction domain (which is common for all modelling teams). We average either (i) over the whole set of values (called Mean) and (ii) for values above the 95th percentile (called P95) as defined here below:</p>
---	--	--

• Mean cell concentration value averaged over time $c_{ij}^{n,k,s} = \frac{1}{T} \sum_{t=1}^T c_{ij,t}^{n,k,s}$ (4)

• 95th percentile concentration value over the domain $c_{P95}^{n,k,s} = 95^{th} \text{Percentile} \{ c_{ij}^{n,k,s} \}$ (5)

• Mean cell concentration value averaged over time and domain $C_{Mean}^{n,k,s} = \frac{1}{I \times J} \sum_{i=1}^I \sum_{j=1}^J c_{ij}^{n,k,s}$ (6)

• Mean concentration value, representing the average of all domain concentrations above the 95th percentile value $C_{P95}^{n,k,s} = c_{ij}^{n,k,s} |_{\forall c_{ij}^{n,k,s} \geq c_{P95}^{n,k,s}}$ (7)

For each averaging type ($ave = Mean$ or $P95$), the following indicators are defined. They are calculated for a given model and for a tuple (n, k, s) representing the pollutant concentrations, the target area and the scenario, respectively. A scenario s is defined as an emission reduction simulation compared with the base case (BC), depending on the percentage of reduction (– 25 or – 50%) over a certain period and type of simulation (LT simulations or ST PM or ST O₃ episodes).

• Absolute impact or delta $\Delta C_{ave}^{n,k,s} = C_{ave}^{n,k,s} - C_{ave}^{n,k,BC}$ (8)

• Relative impact $r\Delta C_{ave}^{n,k,s} = \frac{C_{ave}^{n,k,s} - C_{ave}^{n,k,BC}}{C_{ave}^{n,k,BC}}$ (9)

• Absolute potential – $AbsPTL\alpha$ $APL_{\alpha}^{ave} = \frac{\Delta C_{ave}^{n,k,s}}{\alpha}$ (10)

• Relative potential – $RelPTL\alpha$ $RPL_{\alpha}^{ave} = \frac{APL_{\alpha}^{ave}}{C_{ave}^{n,k,BC}}$ (11)

• Absolute potency – $AbsPTY\alpha$ $APY_{\alpha}^{ave} = \frac{APL_{\alpha}^{ave}}{E_{Total}^{m,k,BC}}$ (12)

The absolute potential is the delta of concentrations normalized by the reduction factor; it represents a potential absolute reduction if a 100% emission reduction assuming linearity. The absolute potency represents the delta normalized by the amount of reduced emissions.

Supplementary Information The online version contains supplementary material available at <https://doi.org/10.1007/s11869-023-01469-z>.

Acknowledgements CIEMAT acknowledges the Ministry for the Ecological Transition and Demographic Challenge for financial support. The WRF-Chem NKUA simulations were supported by computational time granted from the National Infrastructures for Research and Technology S.A. (GRNET S.A.) in the National HPC facility – ARIS –. For LMD, the work was granted access to the HPC resources of TGCC under the allocation 2021- GENI0274 made by GENCI. The computing resources and the related technical support used for the MINNI simulations have been provided by CRESCO/ENEAGRID High Performance Computing infrastructure and its staff. The infrastructure is funded by ENEA, the Italian National Agency for New Technologies,

Energy and Sustainable Economic Development and by Italian and European research programmes (<http://www.cresco.enea.it/english>) and (Iannone et al., 2019). MINNI participation in this project was supported by the “Cooperation Agreement for support to international Conventions, Protocols and related negotiations on air pollution issues”, funded by the Italian Ministry for Environment. The Cyprus Institute acknowledges support from the EMME-CARE project that received funding from the European Union's Horizon 2020 Research and Innovation Programme (under grant agreement no. 856612) and the Cyprus Government, and the LIFE Programme of the European Union in the framework of the project LIFE21-GIE-EL-LIFE-SIR-IUS/101074365. Thanks to FCT/MCTES for the financial support to CESAM (UIDP/50017/2020 + UIDB/50017/2020 + LA/P/0094/2020), through national funds.

Funding -European Union's Horizon 2020 research and innovation program under grant agreement No 874990 (EMERGE project). FCT/MCTES is acknowledged for the financial support to CESAM (UIDP/50017/2020 + UIDB/50017/2020), through national funds.

Data availability All data and the exploration tool are freely available on request.

Declarations

Ethics approval and consent to participate Not applicable.

Consent for publication Not applicable.

Competing interests The authors declare no competing interests.

Open Access This article is licensed under a Creative Commons Attribution 4.0 International License, which permits use, sharing, adaptation, distribution and reproduction in any medium or format, as long as you give appropriate credit to the original author(s) and the source, provide a link to the Creative Commons licence, and indicate if changes were made. The images or other third party material in this article are included in the article's Creative Commons licence, unless indicated otherwise in a credit line to the material. If material is not included in the article's Creative Commons licence and your intended use is not permitted by statutory regulation or exceeds the permitted use, you will need to obtain permission directly from the copyright holder. To view a copy of this licence, visit <http://creativecommons.org/licenses/by/4.0/>.

References

- Ackermann IJ, Hass H, Memmesheimer M, Ebel A, Binkowski FS, Shankar U (1998) Modal aerosol dynamics model for Europe. *Atmos Environ* 32:2981–2999. [https://doi.org/10.1016/S1352-2310\(98\)00006-5](https://doi.org/10.1016/S1352-2310(98)00006-5)
- AIRBASE (2022) Air Quality e-Reporting (AQ e-Reporting) — European Environment Agency [WWW Document]. URL <https://www.eea.europa.eu/data-and-maps/data/aqereporting-9> (accessed 6.18.22)
- ARIANET (2011) SURFPRO3 user's guide (SURFace-atmosphere interface PROCessor, Version 3), Software manual (Software Manual No. R2011.31). ARIANET, Milan, Italy
- Arunachalam S, Holland A, Do B, Abraczinskas M (2006) A quantitative assessment of the influence of grid resolution on predictions of future-year air quality in North Carolina, USA. *Atmos Environ* 40:5010–5026. <https://doi.org/10.1016/j.atmosenv.2006.01.024>
- Baek BH, Seppanen C (2018) SMOKE: SMOKE v4.5 Public Release (April 2017). <https://doi.org/10.5281/zenodo.1321280>
- Bessagnet B, Beauchamp M, Guerreiro C, de Leeuw F, Tsyro S, Colette A, Meleux F, Rouïl L, Ruysenaars P, Sauter F, Velders GJM, Foltescu VL, van Aardenne J (2014a) Can further mitigation of ammonia emissions reduce exceedances of particulate matter air quality standards? *Environ Sci Policy* 44:149–163. <https://doi.org/10.1016/j.envsci.2014.07.011>
- Bessagnet B, Pirovano G, Mircea M, Cuvelier C, Aulinger A, Calori G, Ciarelli G, Manders A, Stern R, Tsyro S, García Vivanco M, Thunis P, Pay M-T, Colette A, Couvidat F, Meleux F, Rouïl L, Ung A, Aksoyoglu S, Baldasano JM, Bieser J, Briganti G, Cappelletti A, D'Isidoro M, Finardi S, Kranenburg R, Silibello C, Carnevale C, Aas W, Dupont J-C, Fagerli H, Gonzalez L, Menut L, Prévôt ASH, Roberts P, White L (2016) Presentation of the EURODELTA III intercomparison exercise – evaluation of the chemistry transport models' performance on criteria pollutants and joint analysis with meteorology. *Atmos Chem Phys* 16:12667–12701. <https://doi.org/10.5194/acp-16-12667-2016>
- Bessagnet B, Colette A, Meleux F, Rouïl L, Ung A, Favez O, Cuvelier C, Thunis P, Tsyro S, Manders A, Kranenburg R, Aulinger A, Bieser J, Mircea M, Briganti G, Cappelletti A, Colari G, Finardi S, Silibello C, Ciarelli G, Aksoyoglu S, Prévôt A, Pay M-T, Baldasano J-M, Garcia Vivanco M, Garrido JL, Palomino I, Martin F, Pirovano G, Roberts P, Gonzalez L, White L, Menut L, Dupont J-C, Carnevale C, Pederzoli A (2014) The EURODELTA III exercise - model evaluation with observations issued from the 2009 EMEP intensive period and standard measurements in Feb/Mar 2009 (No. Report 1/2014). TFMM & MSC-W, Paris, France
- Bessagnet B, Menut L, Lapere R, Couvidat F, Jaffrezo J-L, Maillet S, Favez O, Pennel R, Siour G (2020) High Resolution Chemistry Transport Modeling with the On-Line CHIMERE-WRF Model over the French Alps—Analysis of a Feedback of Surface Particulate Matter Concentrations on Mountain Meteorology. *Atmosphere* 11(6):565. <https://doi.org/10.3390/atmos11060565>
- Binkowski FS, Roselle SJ (2003) Models-3 Community Multiscale Air Quality (CMAQ) model aerosol component 1. Model description. *J Geophys Res* 108:2001JD001409. <https://doi.org/10.1029/2001JD001409>
- Binkowski FS, Shankar U (1995) The Regional Particulate Matter Model: 1. Model description and preliminary results. *J Geophys Res* 100:26191. <https://doi.org/10.1029/95JD02093>
- Boleti E, Hueglin C, Grange SK, Prévôt ASH, Takahama S (2019) Temporal and spatial analysis of ozone concentrations in Europe based on time scale decomposition and a multi-clustering approach (preprint). *Gases/Atmos Model/Troposphere/Chem* (chemical composition and reactions). <https://doi.org/10.5194/acp-2019-909>
- Bossioli E, Tombrou M, Dandou A, Soulakellis N (2007) Simulation of the effects of critical factors on ozone formation and accumulation in the greater Athens area. *J Geophys Res* 112:D02309. <https://doi.org/10.1029/2006JD007185>
- Bossioli E, Sotiropoulou G, Methymaki G, Tombrou M (2021) Modeling extreme warm-air advection in the arctic during summer: the effect of mid-latitude pollution inflow on cloud properties. *JGR Atmospheres* 126:e2020JD033291. <https://doi.org/10.1029/2020JD033291>
- Brands S, Fernández-García G, García Vivanco M, Tesouro Montecelo M, Gallego Fernández N, Saunders Estévez AD, Carracedo García PE, Neto Venâncio A, Melo Da Costa P, Costa Tomé P, Otero C, Macho ML, Taboada J (2020) An exploratory performance assessment of the CHIMERE model (version 2017r4) for the northwestern Iberian Peninsula and the summer season. *Geosci Model Dev* 13:3947–3973. <https://doi.org/10.5194/gmd-13-3947-2020>


- Builtjes PJH, van Loon M, Schaap M, Visschedijk AJH, Bloos JP (2003) Project on the modelling and verification of ozone reduction strategies: contribution of TNO-MEP (TNO report No. MEP-R2003/166). TNO, Apeldoorn, The Netherlands
- Campbell PC, Bash JO, Spero TL (2019) Updates to the Noah land surface model in WRF-CMAQ to improve simulated meteorology, air quality, and deposition. *J Adv Model Earth Syst* 11:231–256. <https://doi.org/10.1029/2018MS001422>
- Carruthers DJ, Holroyd RJ, Hunt JCR, Weng WS, Robins AG, Apsley DD, Thompson DJ, Smith FB (1994) UK-ADMS: a new approach to modelling dispersion in the earth's atmospheric boundary layer. *J Wind Eng Ind Aerodyn* 52:139–153. [https://doi.org/10.1016/0167-6105\(94\)90044-2](https://doi.org/10.1016/0167-6105(94)90044-2)
- Carter WPL, Winer AM, Pitts JN (1982) Effects of kinetic mechanisms and hydrocarbon composition on oxidant-precursor relationships predicted by the ekma isopleth technique. *Atmos Environ* 1967(16):113–120. [https://doi.org/10.1016/0004-6981\(82\)90318-3](https://doi.org/10.1016/0004-6981(82)90318-3)
- Carter, W.P. (2000) Implementation of the SAPRC-99 chemical mechanism into the models-3 framework. Report to the United States Environmental Protection Agency, Washington DC
- Emmons LK, Schwantes RH, Orlando JJ, et al (2020) The Chemistry Mechanism in the Community Earth System Model Version 2 (CESM2). *J Adv Model Earth Syst* 12:e2019MS001882. <https://doi.org/10.1029/2019MS001882>
- Chen F, Dudhia J (2001) Coupling an advanced land surface–hydrology model with the Penn State–NCAR MM5 modeling system. Part I: Model Implementation and Sensitivity. *Mon Wea Rev* 129:569–585. [https://doi.org/10.1175/1520-0493\(2001\)129%3c0569:CAALSH%3e2.0.CO;2](https://doi.org/10.1175/1520-0493(2001)129%3c0569:CAALSH%3e2.0.CO;2)
- Chin M, Ginoux P, Kinne S, Torres O, Holben BN, Duncan BN, Martin RV, Logan JA, Higurashi A, Nakajima T (2002) Tropospheric aerosol optical thickness from the GOCART model and comparisons with satellite and sun photometer measurements. *J Atmos Sci* 59:461–483. [https://doi.org/10.1175/1520-0469\(2002\)059%3c0461:TAOTFT%3e2.0.CO;2](https://doi.org/10.1175/1520-0469(2002)059%3c0461:TAOTFT%3e2.0.CO;2)
- Cholakian A, Bessagnet B, Menut L, et al (2023) Anthropogenic emission scenarios over Europe with the WRF-CHIMERE-v2020 Models: Impact of duration and intensity of reductions on surface concentrations during the winter of 2015. *Atmosphere* 14:224. <https://doi.org/10.3390/atmos14020224>
- Ciarelli G, Theobald MR, Vivanco MG, Beekmann M, Aas W, Andersson C, Bergström R, Manders-Groot A, Couvidat F, Mircea M, Tsyro S, Fagerli H, Mar K, Raffort V, Roustan Y, Pay M-T, Schaap M, Kranenburg R, Adani M, Briganti G, Cappelletti A, D'Isidoro M, Cuvelier C, Cholakian A, Bessagnet B, Wind P, Colette A (2019) Trends of inorganic and organic aerosols and precursor gases in Europe: insights from the EURODELTA multi-model experiment over the 1990–2010 period. *Geosci Model Dev* 12:4923–4954
- Clappier A, Thunis P, Beekmann M, Putaud JP, de Meij A (2021) Impact of SO_x, NO_x and NH₃ emission reductions on PM_{2.5} concentrations across Europe: hints for future measure development. *Environ Int* 156:106699. <https://doi.org/10.1016/j.envint.2021.106699>
- Colette A, Andersson C, Manders A, Mar K, Mircea M, Pay M-T, Raffort V, Tsyro S, Cuvelier C, Adani M, Bessagnet B, Bergström R, Briganti G, Butler T, Cappelletti A, Couvidat F, D'Isidoro M, Doumbia T, Fagerli H, Granier C, Heyes C, Klimont Z, Ojha N, Otero N, Schaap M, Sindelarova K, Stegehuis AI, Roustan Y, Vautard R, Van Meijgaard E, Garcia Vivanco M, Wind P (2017) EURODELTA-Trends, a multi-model experiment of air quality hindcast in Europe over 1990–2010. *Geosci Model Dev* 10:3255–3276
- Crippa M, Guizzardi D, Muntean M, Schaaf E, Dentener F, van Aardenne JA, Monni S, Doering U, Olivier JGJ, Pagliari V, Janssens-Maenhout G (2018) Gridded emissions of air pollutants for the period 1970–2012 within EDGAR v4.3.2. *Earth Syst Sci Data* 10:1987–2013. <https://doi.org/10.5194/essd-10-1987-2018>
- Cuesta J, Costantino L, Beekmann M, Siour G, Menut L, Bessagnet B, Landi TC, Dufour G, Eremenko M (2022) Ozone pollution during the COVID-19 lockdown in the spring of 2020 over Europe, analysed from satellite observations, in situ measurements, and models. *Atmos Chem Phys* 22:4471–4489. <https://doi.org/10.5194/acp-22-4471-2022>
- Curci G (2012) On the impact of time-resolved boundary conditions on the simulation of surface ozone and PM₁₀, in: Khare, M. (Ed.), *Air Pollution - Monitoring, Modelling, Health and Control*. InTech. <https://doi.org/10.5772/33703>
- Cuvelier C, Thunis P, Vautard R, Amann M, Bessagnet B, Bedogni M, Berkowicz R, Brandt J, Brocheton F, Builtjes P, Carnavale C, Coppalle A, Denby B, Douras J, Graf A, Hellmuth O, Hodzic A, Honoré C, Jonson J, Kerschbaumer A, de Leeuw F, Minguzzi E, Moussiopoulos N, Pertot C, Peuch VH, Pirovano G, Rouil L, Sauter F, Schaap M, Stern R, Tarrason L, Vignati E, Volta M, White L, Wind P, Zuber A (2007) CityDelta: a model intercomparison study to explore the impact of emission reductions in European cities in 2010. *Atmos Environ* 41:189–207
- de Meij A, Thunis P, Bessagnet B, Cuvelier C (2009) The sensitivity of the CHIMERE model to emissions reduction scenarios on air quality in Northern Italy. *Atmos Environ* 43:1897–1907
- Denby BR, Gauss M, Wind P, Mu Q, Grötting Wærsted E, Fagerli H, Valdebenito A, Klein H (2020) Description of the uEMEP_v5 downscaling approach for the EMEP MSC-W chemistry transport model. *Geosci Model Dev* 13:6303–6323. <https://doi.org/10.5194/gmd-13-6303-2020>
- Dodge MC (1977) Combined use of modeling techniques and smog chamber data to derive ozone-precursor relationships, in: *Proceedings. Presented at the International Conference on Photochemical Oxidant Pollution and its Control.*, US Environmental Protection Agency, Research Triangle Park, N. C., USA
- Dodge Y (ed) (2006) *The Oxford dictionary of statistical terms*, First published in paperback, 2006th edn. Oxford University Press, Oxford
- Du H, Li J, Wang Z, Yang W, Chen X, Wei Y (2021) Sources of PM_{2.5} and its responses to emission reduction strategies in the Central Plains Economic Region in China: Implications for the impacts of COVID-19. *Environmental Pollution* 288:117783. <https://doi.org/10.1016/j.envpol.2021.117783>
- Dufour G, Hauglustaine D, Zhang Y, Eremenko M, Cohen Y, Gaudel A, Siour G, Lachatre M, Bense A, Bessagnet B, Cuesta J, Ziemke J, Thouret V, Zheng B (2021) Recent ozone trends in the Chinese free troposphere: role of the local emission reductions and meteorology. *Gases/Remote Sens/Troposphere/Chem* (chemical composition and reactions). <https://doi.org/10.5194/acp-2021-476>
- Düring I, Bächlin W, Ketzler M, Baum A, Friedrich U, Wurzler S (2011) A new simplified NO/NO₂ conversion model under consideration of direct NO₂-emissions. *Meteorologische Zeitschrift* 67–73. <https://doi.org/10.1127/0941-2948/2011/0491>
- EEA (2015) *Air quality in Europe: 2015 report*. Publications Office, LU
- EEA (2020) *Air quality in Europe: 2020 report*. Publications Office, LU
- Emmons LK, Walters S, Hess PG, Lamarque J-F, Pfister GG, Fillmore D, Granier C, Guenther A, Kinnison D, Laepple T, Orlando J, Tie X, Tyndall G, Wiedinmyer C, Baughcum SL, Kloster S (2010) Description and evaluation of the Model for Ozone and Related chemical Tracers, version 4 (MOZART-4). *Geosci Model Dev* 3:43–67. <https://doi.org/10.5194/gmd-3-43-2010>
- EU (2008) Directive 2008/50/EC of the European Parliament and of the Council of 21 May 2008 on ambient air quality and cleaner air for Europe (No. OJL 152). European Parliament, Council of the European Union
- Feng R, Fang X (2022) China's pathways to synchronize the emission reductions of air pollutants and greenhouse gases: pros and cons.

- Resour Conserv Recycl 184:106392. <https://doi.org/10.1016/j.resconrec.2022.106392>
- Georgiou GK, Christoudias T, Proestos Y, Kushta J, Hadjinicolaou P, Lelieveld J (2018) Air quality modelling in the summer over the eastern Mediterranean using WRF-Chem: chemistry and aerosol mechanism intercomparison. *Atmos Chem Phys* 18:1555–1571. <https://doi.org/10.5194/acp-18-1555-2018>
- Granier C, Darras S, Denier van der Gon H, Doubalova J, Elguindi N, Galle B, Gauss M, Guevara M, Jalkanen J-P, Kuenen J, Liousse C, Quack B, Simpson D, Sindelarova K (2019) The Copernicus Atmosphere Monitoring Service global and regional emissions (April 2019 version). <https://doi.org/10.24380/D0BN-KX16>
- Grell GA, Dévényi D (2002) A generalized approach to parameterizing convection combining ensemble and data assimilation techniques: parameterizing convection combining ensemble and data assimilation techniques. *Geophys Res Lett* 29:381–384. <https://doi.org/10.1029/2002GL015311>
- Grell GA, Freitas SR (2014) A scale and aerosol aware stochastic convective parameterization for weather and air quality modeling. *Atmos Chem Phys* 14:5233–5250. <https://doi.org/10.5194/acp-14-5233-2014>
- Grell GA, Peckham SE, Schmitz R, McKeen SA, Frost G, Skamarock WC, Eder B (2005) Fully coupled “online” chemistry within the WRF model. *Atmos Environ* 39:6957–6975. <https://doi.org/10.1016/j.atmosenv.2005.04.027>
- Gunther A, Karl T, Harley P, Wiedinmyer C, Palmer PI, Geron C (2006) Estimates of global terrestrial isoprene emissions using MEGAN (Model of Emissions of Gases and Aerosols from Nature). *Atmos Chem Phys* 6:3181–3210. <https://doi.org/10.5194/acp-6-3181-2006>
- Hong S-Y, Noh Y, Dudhia J (2006) A new vertical diffusion package with an explicit treatment of entrainment processes. *Mon Weather Rev* 134:2318–2341. <https://doi.org/10.1175/MWR3199.1>
- Hood C, MacKenzie I, Stocker J, Johnson K, Carruthers D, Vieno M, Doherty R (2018) Air quality simulations for London using a coupled regional-to-local modelling system. *Atmos Chem Phys* 18:11221–11245. <https://doi.org/10.5194/acp-18-11221-2018>
- Huang X, Huang J, Ren C, Wang J, Wang H, Wang J, Yu H, Chen J, Gao J, Ding A (2020) Chemical boundary layer and its impact on air pollution in Northern China. *Environ Sci Technol Lett* 7:826–832. <https://doi.org/10.1021/acs.estlett.0c00755>
- Huertas JI, Martinez DS, Prato DF (2021) Numerical approximation to the effects of the atmospheric stability conditions on the dispersion of pollutants over flat areas. *Sci Rep* 11:11566. <https://doi.org/10.1038/s41598-021-89200-9>
- Iacono MJ, Delamere JS, Mlawer EJ, Shephard MW, Clough SA, Collins WD (2008) Radiative forcing by long-lived greenhouse gases: calculations with the AER radiative transfer models. *J Geophys Res* 113:D13103. <https://doi.org/10.1029/2008JD009944>
- Iannone F, Ambrosino F, Bracco G, De Rosa M, Funel A, Guarnieri G, Migliori S, Palombi F, Ponti G, Santomauro G, Procacci P (2019) CRESCO ENEA HPC clusters: a working example of a multifabric GPFS Spectrum Scale layout, in: 2019 International Conference on High Performance Computing & Simulation (HPCS). Presented at the 2019 International Conference on High Performance Computing & Simulation (HPCS), IEEE, Dublin, Ireland, 1051–1052. <https://doi.org/10.1109/HPCS48598.2019.9188135>
- Im U, Christensen JH, Geels C, Hansen KM, Brandt J, Solazzo E, Alyuz U, Balzarini A, Baro R, Bellasio R, Bianconi R, Bieser J, Colette A, Curci G, Farrow A, Flemming J, Fraser A, Jimenez-Guerrero P, Kitwiroon N, Liu P, Nopmongcol U, Palacios-Peña L, Pirovano G, Pozzoli L, Prank M, Rose R, Sokhi R, Tuccella P, Unal A, Vivanco MG, Yarwood G, Hogrefe C, Galmarini S (2018) Influence of anthropogenic emissions and boundary conditions on multi-model simulations of major air pollutants over Europe and North America in the framework of AQMEII3. *Atmos Chem Phys* 18:8929–8952. <https://doi.org/10.5194/acp-18-8929-2018>
- Janssen S, Dumont G, Fierens F, Mensink C (2008) Spatial interpolation of air pollution measurements using CORINE land cover data. *Atmos Environ* 42:4884–4903. <https://doi.org/10.1016/j.atmosenv.2008.02.043>
- Janssens-Maenhout G, Crippa M, Guizzardi D, Dentener F, Muntean M, Pouliot G, Keating T, Zhang Q, Kurokawa J, Wankmüller R, Denier van der Gon H, Kuenen JJP, Klimont Z, Frost G, Darras S, Koffi B, Li M (2015) HTAP_v2.2: a mosaic of regional and global emission grid maps for 2008 and 2010 to study hemispheric transport of air pollution. *Atmos Chem Phys* 15:11411–11432. <https://doi.org/10.5194/acp-15-11411-2015>
- Janssens-Maenhout G, Crippa M, Guizzardi D, Muntean M, Schaaf E, Dentener F, Bergamaschi P, Pagliari V, Olivier JGJ, Peters JAHW, van Aardenne JA, Monni S, Doering U, Petrescu AMR, Solazzo E, Oreggioni GD (2019) EDGAR v4.3.2 Global Atlas of the three major greenhouse gas emissions for the period 1970–2012. *Earth Syst Sci Data* 11:959–1002. <https://doi.org/10.5194/essd-11-959-2019>
- Khan AW, Kumar P (2019) Impact of chemical initial and lateral boundary conditions on air quality prediction. *Adv Space Res* 64:1331–1342. <https://doi.org/10.1016/j.asr.2019.06.028>
- Kuenen JJP, Visschedijk AJH, Jozwicka M, Denier van der Gon HAC (2014) TNO-MACC_II emission inventory; a multi-year (2003–2009) consistent high-resolution European emission inventory for air quality modelling. *Atmos Chem Phys* 14:10963–10976. <https://doi.org/10.5194/acp-14-10963-2014>
- Kuenen J, Dellaert S, Visschedijk A, Jalkanen J-P, Super I, Denier van der Gon H (2022) CAMS-REG-v4: a state-of-the-art high-resolution European emission inventory for air quality modelling. *Earth Syst Sci Data* 14:491–515. <https://doi.org/10.5194/essd-14-491-2022>
- Kuenen J, Trozi C (2019) EMEP/EEA air pollutant emission inventory guidebook 2019 - Small Combustion. Environment European Agency, Copenhagen, <https://www.eea.europa.eu/publications/emep-eea-guidebook-2019>, DK
- Kushta J, Georgiou GK, Proestos Y, Christoudias T, Thunis P, Savvides C, Papadopoulos C, Lelieveld J (2019) Evaluation of EU air quality standards through modeling and the FAIRMODE benchmarking methodology. *Air Qual Atmos Health* 12:73–86. <https://doi.org/10.1007/s11869-018-0631-z>
- Kushta J, Paisi N, Van Der Gon HD, Lelieveld J (2021) Disease burden and excess mortality from coal-fired power plant emissions in Europe. *Environ Res Lett* 16:045010. <https://doi.org/10.1088/1748-9326/abecff>
- Lapere R, Menut L, Mailler S, Huneeus N (2021) Seasonal variation in atmospheric pollutants transport in central Chile: dynamics and consequences. *Atmos Chem Phys* 21:6431–6454. <https://doi.org/10.5194/acp-21-6431-2021>
- LeGrand SL, Polashenski C, Letcher TW, Creighton GA, Peckham SE, Cetola JD (2019) The AFWA dust emission scheme for the GOCART aerosol model in WRF-Chem v3.8.1. *Geosci Model Dev* 12:131–166. <https://doi.org/10.5194/gmd-12-131-2019>
- Li CWY, Brasseur GP, Schmidt H, Mellado JP (2021) Error induced by neglecting subgrid chemical segregation due to inefficient turbulent mixing in regional chemical-transport models in urban environments. *Atmos Chem Phys* 21:483–503. <https://doi.org/10.5194/acp-21-483-2021>
- Liu P, Hogrefe C, Im U, Christensen JH, Bieser J, Nopmongcol U, Yarwood G, Mathur R, Roselle S, Spero T (2018) Attributing differences in the fate of lateral boundary ozone in AQMEII3 models to physical process representations. *Atmos Chem Phys* 18:17157–17175. <https://doi.org/10.5194/acp-18-17157-2018>
- Maiheu B, Williams ML, Walton HA, Janssen S, Blyth L, Velderman N, Lefebvre W, Vanhulzel M, Bevers SD (2017) Improved

- methodologies for NO₂ exposure assessment in the EU (Vito Report No. 2017/RMA/R/150)
- Mailler S, Menut L, Khvorostyanov D, Valari M, Couvidat F, Siour G, Turquety S, Briant R, Tuccella P, Bessagnet B, Colette A, Létinois L, Markakis K, Meleux F (2017) CHIMERE-2017: from urban to hemispheric chemistry-transport modeling. *Geosci Model Dev* 10:2397–2423. <https://doi.org/10.5194/gmd-10-2397-2017>
- Manders AMM, Builtjes PJH, Curier L, Denier van der Gon HAC, Hendriks C, Jonkers S, Kranenburg R, Kuenen JJP, Segers AJ, Timmermans RMA, Visschedijk AJH, Wichink Kruit RJ, van Pul WAJ, Sauter FJ, van der Swaluw E, Swart DPJ, Douros J, Eskes H, van Meijgaard E, van Ulft B, van Velthoven P, Banzhaf S, Mues AC, Stern R, Fu G, Lu S, Heemink A, van Velzen N, Schaap M (2017) Curriculum vitae of the LOTOS-EUROS (v2.0) chemistry transport model. *Geosci Model Dev* 10:4145–4173. <https://doi.org/10.5194/gmd-10-4145-2017>
- Mao Y-H, Yu S, Shang Y, Liao H, Li N (2022) Response of summer ozone to precursor emission controls in the Yangtze River Delta Region. *Front Environ Sci* 10:864897. <https://doi.org/10.3389/fenvs.2022.864897>
- Mareckova K, Pinteris M, Ullrich B, Wankmueller R, Gaisbauer S (2019) Review of emission data reported under the LRTAP Convention and the NEC Directive Stage 1 and 2 review Status of gridded and LPS data (EMEP report No. 4/2019). Umweltbundesamt GmbH, Vienna, Austria
- Menut L, Bessagnet B, Briant R, Cholokian A, Couvidat F, Mailler S, Pennel R, Siour G, Tuccella P, Turquety S, Valari M (2021) The CHIMERE v2020r1 online chemistry-transport model. *Geosci Model Dev* 14:6781–6811. <https://doi.org/10.5194/gmd-14-6781-2021>
- Menut L, Bessagnet B, Siour G, Mailler S, Pennel R, Cholokian A (2020) Impact of lockdown measures to combat Covid-19 on air quality over western Europe. *Sci Total Environ* 741:140426. <https://doi.org/10.1016/j.scitotenv.2020.140426>
- Miglietta MM, Thunis P, Georgieva E, Pederzoli A, Bessagnet B, Terrenoire E, Colette A (2012) Evaluation of WRF model performance in different European regions with the DELTA-FAIRMODE evaluation tool. *Int J Environ Pollut* 50:83–97
- Mircea M, Ciancarella L, Briganti G, Calori G, Cappelletti A, Cionni I, Costa M, Cremona G, D'Isidoro M, Finardi S, Pace G, Piersanti A, Righini G, Silibello C, Vitali L, Zanini G (2014) Assessment of the AMS-MINNI system capabilities to simulate air quality over Italy for the calendar year 2005. *Atmos Environ* 84:178–188. <https://doi.org/10.1016/j.atmosenv.2013.11.006>
- Mircea M, Grigoras G, D'Isidoro M, Righini G, Adani M, Briganti G, Ciancarella L, Cappelletti A, Calori G, Cionni I, Cremona G, Finardi S, Larsen BR, Pace G, Perrino C, Piersanti A, Silibello C, Vitali L, Zanini G (2016) Impact of grid resolution on aerosol predictions: a case study over Italy. *Aerosol Air Qual Res* 16:1253–1267. <https://doi.org/10.4209/aaqr.2015.02.0058>
- Mircea M, Bessagnet B, D'Isidoro M, Pirovano G, Aksoyoglu S, Ciarelli G, Tsyro S, Manders A, Bieser J, Stern R, Vivanco MG, Cuvelier C, Aas W, Prévôt ASH, Aulinger A, Briganti G, Calori G, Cappelletti A, Colette A, Couvidat F, Fagerli H, Finardi S, Kranenburg R, Rouil L, Silibello C, Spindler G, Poulain L, Herrmann H, Jimenez JL, Day DA, Tiitta P, Carbone S (2019) EURODELTA III exercise: An evaluation of air quality models' capacity to reproduce the carbonaceous aerosol. *Atmos Environ X* 2:100018. <https://doi.org/10.1016/j.aeaoa.2019.100018>
- Mlawer EJ, Taubman SJ, Brown PD, Iacono MJ, Clough SA (1997) Radiative transfer for inhomogeneous atmospheres: RRTM, a validated correlated-k model for the longwave. *J Geophys Res* 102:16663–16682. <https://doi.org/10.1029/97JD00237>
- Monteiro A, Durka P, Flandorfer C, Georgieva E, Guerreiro C, Kushta J, Malherbe L, Maiheu B, Miranda AI, Santos G, Stocker J, Trimpe-neers E, Tognet F, Stortini M, Wesseling J, Janssen S, Thunis P (2018) Strengths and weaknesses of the FAIRMODE benchmarking methodology for the evaluation of air quality models. *Air Qual Atmos Health* 11:373–383. <https://doi.org/10.1007/s11869-018-0554-8>
- Morrison H, Curry JA, Shupe MD, Zuidema P (2005) A new double-moment microphysics parameterization for application in cloud and climate models. Part II: Single-column modeling of Arctic clouds. *J Atmos Sci* 62:1678–1693. <https://doi.org/10.1175/JAS3447.1>
- Mu Q, Denby BR, Wærsted EG, Fagerli H (2022) Downscaling of air pollutants in Europe using uEMEP_v6. *Geosci Model Dev* 15:449–465. <https://doi.org/10.5194/gmd-15-449-2022>
- Nakanishi M, Niino H (2006) An improved Mellor-Yamada Level-3 model: its numerical stability and application to a regional prediction of advection fog. *Boundary-Layer Meteorol* 119:397–407. <https://doi.org/10.1007/s10546-005-9030-8>
- NCEP (2015) NCEP GDAS/FNL 0.25 degree global tropospheric analyses and forecast grids. <https://doi.org/10.5065/D65Q4T4Z>
- Nenes A, Pandis SN, Pilinis C (1998) ISORROPIA: a new thermodynamic model for multiphase multicomponent inorganic aerosols. *Aquat Geochem* 4:123–152. <https://doi.org/10.1023/A:1009604003981>
- Ntziachristos L, Boulter P (2019) EMEP/EEA air pollutant emission inventory guidebook 2019 - 1.A.3.b.vi Road transport: Automobile tyre and brake wear - 1.A.3.b.vii Road transport: Automobile road abrasion. European Environment Agency
- OECD (2012) Redefining “urban”: a new way to measure metropolitan areas. OECD, Paris
- Oke TR, Mills G, Christen A, Voegt JA (2017) Urban climates. Cambridge University Press Cambridge. <https://doi.org/10.1017/9781139016476>
- Oreggioni GD, Monforti Ferraio F, Crippa M, Muntean M, Schaaf E, Guizzardi D, Solazzo E, Duerr M, Perry M, Vignati E (2021) Climate change in a changing world: socio-economic and technological transitions, regulatory frameworks and trends on global greenhouse gas emissions from EDGAR v.5.0. *Glob Environ Chang* 70:102350. <https://doi.org/10.1016/j.gloenvcha.2021.102350>
- Otte TL, Pouliot G, Pleim JE, Young JO, Schere KL, Wong DC, Lee PCS, Tsidulko M, McQueen JT, Davidson P, Mathur R, Chuang H-Y, DiMego G, Seaman NL (2005) Linking the Eta model with the Community Multiscale Air Quality (CMAQ) modeling system to build a national air quality forecasting system. *Weather Forecast* 20:367–384. <https://doi.org/10.1175/WAF855.1>
- Owens R, Hewson T (2018) ECMWF Forecast User Guide. <https://doi.org/10.21957/M1CS7H>
- Pernigotti D, Georgieva E, Thunis P, Bessagnet B (2012) Impact of meteorology on air quality modeling over the Po valley in northern Italy. *Atmos Environ* 51:303–310
- Petetin H, Sciare J, Bressi M, Gros V, Rosso A, Sanchez O, Sarda-Estève R, Petit J-E, Beekmann M (2016) Assessing the ammonium nitrate formation regime in the Paris megacity and its representation in the CHIMERE model. *Atmos Chem Phys* 16:10419–10440. <https://doi.org/10.5194/acp-16-10419-2016>
- Pisoni E, Guerreiro C, Lopez-Aparicio S, Guevara M, Tarrason L, Janssen S, Thunis P, Pfäfflin F, Piersanti A, Briganti G, Cappelletti A, D'Elia I, Mircea M, Villani MG, Vitali L, Matavž L, Rus M, Žabkar R, Kauhaniemi M, Karppinen A, Kousa A, Väkevä O, Eneroth K, Stortini M, Delaney K, Struzewska J, Durka P, Kaminski JW, Krmpotic S, Vidic S, Belavic M, Brzoja D, Milic V, Assimakopoulos VD, Fameli KM, Polimerova T, Stoyneva E, Hristova Y, Sokolovski E, Cuvelier C (2019) Supporting the improvement of air quality management practices: the “FAIRMODE pilot” activity. *J Environ Manage* 245:122–130. <https://doi.org/10.1016/j.jenvman.2019.04.118>
- Schell B, Ackermann IJ, Hass H, Binkowski FS, Ebel A (2001) Modeling the formation of secondary organic aerosol within a comprehensive air quality model system. *J Geophys Res* 106:28275–28293. <https://doi.org/10.1029/2001JD000384>

- Silibello C, Calori G, Brusasca G, Giudici A, Angelino E, Fossati G, Peroni E, Buganza E (2008) Modelling of PM10 concentrations over Milano urban area using two aerosol modules. *Environ Model Softw* 23:333–343. <https://doi.org/10.1016/j.envsoft.2007.04.002>
- Simpson D, Benedictow A, Berge H, Bergström R, Emberson LD, Fagerli H, Flechard CR, Hayman GD, Gauss M, Jonson JE, Jenkin ME, Nyíri A, Richter C, Semeena VS, Tsyro S, Tuovinen J-P, Valdebenito Á, Wind P (2012) The EMEP MSC-W chemical transport model – technical description. *Atmos Chem Phys* 12:7825–7865. <https://doi.org/10.5194/acp-12-7825-2012>
- Skamarock W, Klemp J, Dudhia J, Gill D, Barker D, Wang W, Huang X-Y, Duda M (2008) A description of the advanced research WRF version 3. UCAR/NCAR. <https://doi.org/10.5065/D68S4MVH>
- Solazzo E, Bianconi R, Pirovano G, Matthias V, Vautard R, Moran MD, Appel KW, Bessagnet B, Brandt J, Christensen JH, Chemel C, Coll I, Ferreira J, Forkel R, Francis XV, Grell G, Grossi P, Hansen AB, Miranda AI, Nopmongcol U, Prank M, Sartelet KN, Schaap M, Silver JD, Sokhi RS, Vira J, Werhahn J, Wolke R, Yarwood G, Zhang J, Rao ST, Galmarini S (2012) Operational model evaluation for particulate matter in Europe and North America in the context of AQMEII. *Atmos Environ* 53:75–92
- Solazzo E, Bianconi R, Pirovano G, Moran MD, Vautard R, Hogrefe C, Appel KW, Matthias V, Grossi P, Bessagnet B, Brandt J, Chemel C, Christensen JH, Forkel R, Francis XV, Hansen AB, McKeen S, Nopmongcol U, Prank M, Sartelet KN, Segers A, Silver JD, Yarwood G, Werhahn J, Zhang J, Rao ST, Galmarini S (2013) Evaluating the capability of regional-scale air quality models to capture the vertical distribution of pollutants. *Geosci Model Dev* 6:791–818
- Stockwell WR, Middleton P, Chang JS, Tang X (1990) The second generation regional acid deposition model chemical mechanism for regional air quality modeling. *J Geophys Res* 95:16343. <https://doi.org/10.1029/JD095iD10p16343>
- Stockwell WR, Kirchner F, Kuhn M, Seefeld S (1997) A new mechanism for regional atmospheric chemistry modeling. *J Geophys Res* 102:25847–25879. <https://doi.org/10.1029/97JD00849>
- Thunis P, Clappier A (2014) Indicators to support the dynamic evaluation of air quality models. *Atmos Environ* 98:402–409. <https://doi.org/10.1016/j.atmosenv.2014.09.016>
- Thunis P, Rouil L, Cuvelier C, Stern R, Kerschbaumer A, Bessagnet B, Schaap M, Builtjes P, Tarrason L, Douros J, Moussiopoulos N, Pirovano G, Bedogni M (2007) Analysis of model responses to emission-reduction scenarios within the CityDelta project. *Atmos Environ* 41:208–220
- Thunis P, Cuvelier C, Roberts P, White L, Nyri A, Stern R, Kerschbaumer A, Bessagnet B, Bergström R, Schaap M (2010) EURODELTA : evaluation of a sectoral approach to integrated assessment modelling : second report. Publications Office, LU
- Thunis P, Pisoni E, Degraeuwe B, Kranenburg R, Schaap M, Clappier A (2015) Dynamic evaluation of air quality models over European regions. *Atmos Environ* 111:185–194. <https://doi.org/10.1016/j.atmosenv.2015.04.016>
- Thunis P, Clappier A, Beekmann M, Putaud JP, Cuvelier C, Madrazo J, de Meij A (2021a) Non-linear response of PM2.5; to changes in NO2; and NH3 emissions in the Po basin (Italy): consequences for air quality plans. *Atmos Chem Phys* 21:9309–9327. <https://doi.org/10.5194/acp-21-9309-2021>
- Thunis P, Crippa M, Cuvelier C, Guizzardi D, de Meij A, Oreggioni G, Pisoni E (2021b) Sensitivity of air quality modelling to different emission inventories: a case study over Europe. *Atmos Environ: X* 10:100111. <https://doi.org/10.1016/j.aea.2021.100111>
- Tilmes S, Hodzic A, Emmons LK, Mills MJ, Gettelman A, Kinnison DE, Park M, Lamarque J-F, Vitt F, Shrivastava M, Campuzano-Jost P, Jimenez JL, Liu X (2019) Climate forcing and trends of organic aerosols in the Community Earth System Model (CESM2). *J Adv Model Earth Syst* 11:4323–4351. <https://doi.org/10.1029/2019MS001827>
- UNECE (2013) ECE/EB.AIR/114 - 1999 Protocol to abate acidification, eutrophication and ground-level ozone to the convention on longrange transboundary air pollution, as amended on 4 May 2012
- US EPA Office of Research and Development (2020) CMAQ. <https://doi.org/10.5281/zenodo.4081737>
- Vautard R, Builtjes PHJ, Thunis P, Cuvelier C, Bedogni M, Bessagnet B, Honoré C, Moussiopoulos N, Pirovano G, Schaap M, Stern R, Tarrason L, Wind P (2007) Evaluation and intercomparison of ozone and PM10 simulations by several chemistry transport models over four European cities within the CityDelta project. *Atmos Environ* 41:173–188
- Viaene P, Belis CA, Blond N, Bouland C, Juda-Rezler K, Karvonenja N, Martilli A, Miranda A, Pisoni E, Volta M (2016) Air quality integrated assessment modelling in the context of EU policy: a way forward. *Environ Sci Policy* 65:22–28. <https://doi.org/10.1016/j.envsci.2016.05.024>
- Vitali L, Adani M, Briganti G, Ciancarella L, Cremona G, D'Elia I, Guarnieri G, D'Isidoro M, Mircea M, Piersanti A, Righini A, Russo F, Villani MG, Zanini G (2019) AMS-MINNI National air quality simulation on Italy for the calendar year 2015 (Technical report No. RT/2019/15/ENEA). ENEA
- Vivanco MG, Correa M, Azula O, Palomino I, Martín F (2008) Influence of model resolution on ozone predictions over Madrid Area (Spain). In: Gervasi O, Murgante B, Laganà A, Taniar D, Mun Y, Gavrilova ML (eds) *Computational science and its applications – ICCSA 2008*. Springer, Berlin Heidelberg, Berlin, Heidelberg, pp 165–178
- Vivanco MG, Palomino I, Vautard R, Bessagnet B, Martin F, Menut L, Jimenez S (2009) Multi-year assessment of photochemical air quality simulation over Spain. *Environ Model Softw* 24:63–73
- Vivanco MG, Bessagnet B, Cuvelier C, Theobald MR, Tsyro S, Pirovano G, Aulinger A, Bieser J, Calori G, Ciarelli G, Manders A, Mircea M, Aksoyoglu S, Briganti G, Cappelletti A, Colette A, Couvidat F, D'Isidoro M, Kranenburg R, Meleux F, Menut L, Pay MT, Rouil L, Silibello C, Thunis P, Ung A (2017) Joint analysis of deposition fluxes and atmospheric concentrations of inorganic nitrogen and sulphur compounds predicted by six chemistry transport models in the frame of the EURODEL-TAII project. *Atmos Environ* 151:152–175
- Vivanco MG, Garrido JL, Martín F, Theobald MR, Gil V, Santiago J-L, Lechón Y, Gamarra AR, Sánchez E, Alberto A, Bailador A (2021) Assessment of the effects of the Spanish national air pollution control programme on air quality. *Atmosphere* 12:158. <https://doi.org/10.3390/atmos12020158>
- Vuolo MR, Menut L, Chepfer H (2009) Impact of transport schemes on modeled dust concentrations. *J Atmos Oceanic Tech* 26:1135–1143. <https://doi.org/10.1175/2008JTECHA1197.1>
- Wesely ML (1989) Parameterization of surface resistances to gaseous dry deposition in regional-scale numerical models. *Atmos Environ* 1967(23):1293–1304. [https://doi.org/10.1016/0004-6981\(89\)90153-4](https://doi.org/10.1016/0004-6981(89)90153-4)
- Xu H, Chen H (2021) Impact of urban morphology on the spatial and temporal distribution of PM2.5 concentration: a numerical simulation with WRF/CMAQ model in Wuhan, China. *J Environ Manag* 290:112427. <https://doi.org/10.1016/j.jenvman.2021.112427>
- Yan F, Gao Y, Ma M, Liu C, Ji X, Zhao F, Yao X, Gao H (2021) Revealing the modulation of boundary conditions and governing processes on ozone formation over northern China in June 2017. *Environ Pollut* 272:115999. <https://doi.org/10.1016/j.envpol.2020.115999>
- Zhou D, Ding K, Huang X, Liu L, Liu Q, Xu Z, Jiang F, Fu C, Ding A (2018) Transport, mixing and feedback of dust, biomass burning and anthropogenic pollutants in eastern Asia: a case study. *Atmos Chem Phys* 18:16345–16361. <https://doi.org/10.5194/acp-18-16345-2018>

Authors and Affiliations

Bertrand Bessagnet¹  · Kees Cuvelier¹ · Alexander de Meij² · Alexandra Monteiro³ · Enrico Pisoni¹ · Philippe Thunis¹ · Angelos Violaris⁴ · Jonilda Kushta⁴ · Bruce R. Denby⁵ · Qing Mu⁵ · Eivind G. Wærsted⁵ · Marta G. Vivanco⁶ · Mark R. Theobald⁶ · Victoria Gil⁶ · Ranjeet S. Sokhi⁷ · Kester Momoh⁷ · Ummugulsum Alyuz⁷ · Rajasree VPM⁷ · Saurabh Kumar⁷ · Elissavet Bossioli⁸ · Georgia Methymaki⁸ · Darijo Brzoja⁹ · Velimir Milić⁹ · Arineh Cholakian¹⁰ · Romain Pennel¹⁰ · Sylvain Mailler¹⁰ · Laurent Menut¹⁰ · Gino Briganti¹¹ · Mihaela Mircea¹¹ · Claudia Flandorfer¹² · Kathrin Baumann-Stanzer¹² · Virginie Hutsemékers¹³ · Elke Trimpeneers¹³

✉ Bertrand Bessagnet
bertrand.bessagnet@ec.europa.eu

¹ European Commission, Joint Research Centre (JRC), Ispra, Italy

² MetClim, Varese, Italy

³ CESAM, Department of Environment and Planning, University of Aveiro, 3810-193 Aveiro, Portugal

⁴ The Cyprus Institute, Climate and Atmosphere Research Center (CARE-C), 20 Konstantinou Kavafi Street, 2121 Nicosia, Cyprus

⁵ Norwegian Meteorological Institute, Henrik Mohns Plass 1, 0313 Oslo, Norway

⁶ Atmospheric Modelling Unit, Environment Department, CIEMAT - Avda. Complutense, 40, 28040 Madrid, Spain

⁷ Centre for Climate Change Research (C3R), School of Physics, Engineering and Computing Science, University of Hertfordshire, College Lane, Hatfield AL10 9AB, UK

⁸ Department of Physics, Sector of Environmental Physics & Meteorology, National and Kapodistrian University of Athens, Athens, Greece

⁹ Croatian Meteorological and Hydrological Service, Ravnice 48, 10000 Zagreb, Croatia

¹⁰ Laboratoire de Météorologie Dynamique (LMD), Ecole Polytechnique, IPSL Research University, Ecole Normale Supérieure, Université Paris-Saclay, Sorbonne Universités, UPMC Univ Paris 06, CNRS, Route de Saclay, 91128 Palaiseau, France

¹¹ ENEA – National Agency for New Technologies, Energy and Sustainable Economic Development, Via Martiri Di Monte Sole, 4, 40129 Bologna, Italy

¹² GeoSphere Austria, Hohe Warte 38, 1190 Vienna, Austria

¹³ Belgian Interregional Environment Agency, Rue Gaucheret 92-94, 1030 Brussels, Belgium